Intercomparison of methods to estimate GPP based on CO_2 and COS flux measurements

Kukka-Maaria Kohonen[1], Roderick Dewar[1,2], Gianluca Tramontana[3,4], Aleksanteri Mauranen[1],
Pasi Kolari[1], Linda M.J. Kooijmans[5], Dario Papale[6,7], Timo Vesala[1,8,9], and Ivan Mammarella[1]

[1]Institute for Atmospheric and Earth System Research/ Physics, Faculty of Science, University of Helsinki, Helsinki, Finland
[2]Plant Sciences Division, Research School of Biology, The Australian National University, Canberra, ACT 2601, Australia
[3]Image Processing Laboratory (IPL), Parc Científic Universitat de València, Universitat de València, Paterna, Spain
[4]Terrasystem s.r.l, Viterbo, Italy
[5]Meteorology and Air Quality, Wageningen University and Research, Wageningen, The Netherlands
[6]DIBAF, Department for Innovation in Biological, Agro-food and Forestry Systems, University of Tuscia, Viterbo, Italy
[7]IAFES, Euro-Mediterranean Center on Climate Change (CMCC), Viterbo, Italy
[8]Institute for Atmospheric and Earth System Research / Forest Sciences, University of Helsinki, Helsinki, Finland
[9]Yugra State University, 628012, Khanty-Mansiysk, Russia

Correspondence: Kukka-Maaria Kohonen (kukka-maaria.kohonen@helsinki.fi)

Abstract. Knowing the components of ecosystem scale carbon exchange is crucial in order to develop better models and future predictions of the terrestrial carbon cycle. However, there are several uncertainties and unknowns related to current photosynthesis estimates. In this study, we test the use of four different methods for quantifying photosynthesis at the ecosystem scale, of which two are based on carbon dioxide (CO_2) and two on carbonyl sulfide (COS) flux measurements. The CO_2-

5 based methods use traditional flux partitioning and artificial neural networks to separate the net CO_2 flux into respiration and photosynthesis. The COS-based methods make use of a unique five year COS flux data set at a boreal forest and include two different approaches to determine the leaf scale uptake ratio of COS and CO_2 (LRU), of which one (LRU_{CAP}) was developed in this study. LRU_{CAP} was based on stomatal conductance theories, while the other was based on an empirical relation to measured radiation (LRU_{PAR}).

10 We found that for the measurement period 2013–2017 the artificial neural networks method gave a GPP estimate very close to that of traditional flux partitioning at all time scales. COS-based methods gave on average higher GPP estimates than the CO_2-based estimates on daily (23 and 7 % higher, if using LRU_{PAR} or LRU_{CAP} in GPP calculation, respectively) and monthly scales (20 and 3 % higher), as well as a higher cumulative sum over three months in all years (on average 25 and 3 % higher). LRU_{CAP} was higher than measured LRU at high radiation leading to an underestimated GPP during midday. However, in

15 general it compared better with the CO_2-based methods than LRU_{PAR}-based GPP calculations. The applicability of LRU_{CAP} at other measurement sites is potentially better than that of LRU_{PAR} since its parameters are based on literature values and simple meteorological measurements, while the radiation relation in LRU_{PAR} might be site-specific. This, however, requires further testing at other measurement sites.

1 Introduction

Photosynthetic carbon uptake (described by gross primary production, GPP) is a crucial part of carbon cycling and removes approximately 30 % of the annual anthropogenic carbon dioxide (CO_2) emissions from the atmosphere (Luo et al., 2015; Friedlingstein et al., 2020). With the current climatic warming it is suggested that both photosynthesis and respiration are increased, due to a CO_2 fertilization effect and rising temperatures allowing more optimal conditions for photosynthesis but also for respiration (Dusenge et al., 2019). However, it is not known at which ratio these two processes are changing and whether they cancel each other out or not. In addition, there is a seasonal variation in their relative importance, as photosynthesis is predicted to increase more than respiration in spring, causing greater carbon uptake, while respiration is predicted to increase more than photosynthesis in autumn, causing carbon emissions in the northern terrestrial ecosystems (Piao et al., 2008). Methods to measure and study photosynthesis and respiration processes individually are thus crucial for future carbon cycle predictions.

Eddy covariance (EC) is widely used globally to measure the biosphere-atmosphere exchange of CO_2 at the ecosystem scale. With EC it is, however, only possible to measure the net ecosystem CO_2 flux (NEE), which includes contributions from both the CO_2 uptake by photosynthesis (GPP) as well as ecosystem respiration (R). NEE partitioning into GPP and respiration is most commonly done using a method introduced by Reichstein et al. (2005), in which temperature response curves are fitted to nighttime CO_2 flux data (respiration). However, this method is problematic due to the reliance on nighttime EC flux measurements, which are uncertain and often filtered out due to low turbulence conditions and possible advective gas transport (Aubinet, 2008). Partitioning methods that are based on a combination of nighttime respiration temperature response (nighttime method) and daytime GPP radiation response (daytime method) have also been developed in order to not rely on nighttime responses only (Lasslop et al., 2010; Kulmala et al., 2019). Both the nighttime method and the combination of nighttime and daytime methods, however, assume that the respiratory processes are the same in the daytime and nighttime and have uncertainties due to assumptions of functional relationships (Tramontana et al., 2020). These limitations lead to uncertainties in the derivation of mechanistically sound descriptions of respiration and its drivers, especially when contributions of different biomass compartments to total CO_2 efflux vary across ecosystems and seasonally even within one ecosystem (Kolari et al., 2009; Keenan et al., 2019). Recently, there has been discussion on leaf respiration inhibition under radiation, the so-called Kok effect (Kok, 1949; Heskel et al., 2013; Yin et al., 2020). Keenan et al. (2019) and Wehr et al. (2016) also suggest that the global GPP estimates based on the nighttime method are exaggerated due to this phenomenon. On the other hand, photorespiration, which is an oxidation process competing with carboxylation under radiation, might cancel out the inhibition by the Kok effect (Heskel et al., 2013).

One way to address biases related to flux partitioning is using machine learning methods, such as artificial neural networks in separating NEE into respiration and GPP (Tramontana et al., 2020). The benefit of NN_{C-part} is that it requires no predefined knowledge on responses to environmental drivers but determines them purely based on data. A pioneering experiment from Desai et al. (2008), attempted to use artificial neural network to emulate the nighttime partitioning method without significant

improvements. Recently a new approach (NN_{C-part}) has been proposed by Tramontana et al. (2020). The proposed method is innovative for the peculiarity of the implemented network's structure and a novel way to infer GPP and R signals from NEE. Both nighttime and daytime NEE are used for network training, so the dynamics of biophysical processes are accounted in a

55   comprehensive way.

Another recent development to tackle the GPP problem is to use proxies for CO_2 uptake. One such proxy is carbonyl sulfide (COS), which is a sulfur compound with a tropospheric mixing ratio around 500 ppt (Montzka et al., 2007). It is mainly produced by oceans and anthropogenic sources (Kettle et al., 2002; Berry et al., 2013; Launois et al., 2015; Whelan et al., 2018) while vegetation is the largest sink (Sandoval-Soto et al., 2005; Blonquist et al., 2011). COS has been suggested as a

60   proxy for GPP since it is taken up by plants through the same diffusive pathway as CO_2 and transported to the chloroplast surface, where it is destroyed by a hydrolysis reaction triggered by the enzyme carbonic anhydrase (CA), while CO_2 continues its journey inside the chloroplast, where it is assimilated in the Calvin cycle (Wohlfahrt et al., 2012). It is assumed that COS is totally destroyed in hydrolysis and thus there is no back-flux from the leaf to the atmosphere (Protoschill-Krebs et al., 1996). When determining GPP from COS flux measurements one needs to take into account the leaf relative uptake ratio (LRU), that

65   is, the ratio of COS and CO_2 deposition rates at the leaf scale. While LRU has been treated either as a global or plant-specific constant value in the past (Asaf et al., 2013; Stimler et al., 2012), recent studies have shown that LRU is a function of solar radiation because CO_2 uptake is highly radiation dependent while COS uptake is not (Yang et al., 2018; Kooijmans et al., 2019; Spielmann et al., 2019), and could even vary with vapour pressure deficit (Sun et al., 2018b; Kooijmans et al., 2019). In addition to uncertainties related to LRU, the COS-based GPP estimates have uncertainty due to ecosystem scale COS flux

70   measurements that typically have a low signal-to-noise ratio and high random uncertainty at 30 min timescale, which reduces when fluxes are averaged over longer time periods (Kohonen et al., 2020). While the use of different partitioning methods or machine learning in GPP calculation primarily aims at more accurate GPP estimation, the use of COS as a GPP proxy aims at a better process understanding.

In this study, we compare the annual, seasonal, daily and sub-daily variation of i) traditionally partitioned GPP (GPP_{NLR},

75   NLR referring to non-linear regressions) that is based on a combination of the daytime and nighttime methods, ii) a GPP estimate based on NEE and NN_{C-part} (GPP_{ANN}), iii) a GPP estimate from COS flux measurements using the radiation-dependent LRU function from Kooijmans et al. (2019) ($GPP_{COS,PAR}$) and iv) a GPP estimate from COS flux measurements using a new, theory-based method for LRU calculation ($GPP_{COS,CAP}$) in a boreal evergreen needle-leaf forest during years 2013–2017. Our aim is to study inconsistencies in diel or seasonal patterns of GPP which could arise from the extrapolation of

80   temperature responses to daytime and discuss the limitations and uncertainties of all four methods.

2   Materials and methods

2.1   Site description

The measurements were done at the Hyytiälä forest Station for Measuring Ecosystem Atmosphere Relations (SMEAR) II measurement site (61°51'N, 24°17'E), where first flux measurements started in 1996 while the forest stand is already more

85 than 50 years old (Hari and Kulmala, 2005). The forest stand is dominated by Scots Pine (*Pinus Sylvestris L.*) with some Norway spruce (*Picea abies L. Karst.*) and deciduous trees (e.g. *Betula sp., Populus tremula, Sorbus aucuparia*). The daytime flux footprint covers c. 50 ha area of the forest. The canopy height increased from approximately 18 to 20 m during the measurement period (2013–2017) and the all-sided leaf area index (LAI) was c. 8 m^2 m^{-2}.

2.2 Measurements

2.2.1 Eddy covariance fluxes and environmental measurements

90

EC measurements were conducted at a 23 m high tower. The setup consisted of Gill HS (Gill Instruments Ltd., England, UK) sonic anemometer measuring horizontal and vertical wind velocities and sonic temperature, and a quantum cascade laser (QCL; Aerodyne Research Inc., Billerica, MA, USA) for measuring COS, CO_2 and H_2O mixing ratios at 10 Hz frequency. The setup is described in more detail in Kohonen et al. (2020) and flux data presented in Vesala et al. (2021). Flux processing was done using

95 EddyUH software (Mammarella et al., 2016) following the methods presented by Kohonen et al. (2020). Fluxes were corrected for storage change and filtered according to friction velocity. Storage change fluxes of COS were calculated from the COS profile measurements in 2015–2017 and from one level concentration measurement in other years, as described in Kohonen et al. (2020), while CO_2 storage change fluxes were calculated from CO_2 concentration profile measurements. The friction velocity threshold was determined from CO_2 fluxes (Papale et al., 2006) and a threshold of 0.3 m s^{-1} was applied to the whole

100 data set to exclude time periods with low turbulence. COS flux processing was done otherwise similarly to CO_2 processing, but time lag and spectral corrections were determined from CO_2 measurements and applied to COS as recommended in Kohonen et al. (2020). Gap-filling of the COS flux was done using empirical formulas based on photosynthetically active radiation (PAR) and vapor pressure deficit (VPD), described in Kohonen et al. (2020). CO_2 fluxes were gap-filled and partitioned with a procedure explained in more detail in Sect. 2.3.1.

105 Environmental measurements used in the study include air temperature (T_a) at 16.8 m (measured with a Pt100 temperature sensor inside a custom shield), PAR above the canopy (Li-190SZ quantum sensor, LI-COR, Lincoln, NE, USA), relative humidity (RH) at 16.8 m height (Rotronic MP102H, Rotronic Instrument Corp., NY, USA), soil temperature (T_{soil}) at 2–5 cm depth (KTY81-110 temperature sensor, Philips, The Netherlands) as a mean of five locations and soil water content (SWC) in the humus layer (Delta-T ML2 soil moisture sensor, Delta-T Devices, Cambridge, UK).

2.3 GPP calculations

110

In this section, all used GPP calculation methods are explained in detail. Daily average GPP was only calculated if more than 50% of measured flux data was available for each day and monthly averages calculated from these data. Gap-filled flux data were used in diurnal variation and in calculating the cumulative GPP. All comparisons between the methods were done to measured (non gap-filled) data only, when both CO_2 and COS flux data were available.

2.3.1 GPP from traditional CO_2 flux partitioning

NEE was partitioned into respiration (R) and GPP_{NLR} as

$$NEE = R - GPP_{NLR} \tag{1}$$

where the GPP model followed the formula

$$GPP_{NLR} = \frac{\alpha PAR + P_{max} - \sqrt{(\alpha PAR + P_{max})^2 - 4\Theta PAR \cdot P_{max}}}{2\Theta} f(T_a) \tag{2}$$

where α, P_{max} and Θ are fitting parameters and $f(T_a)$ an instantaneous temperature response that forces GPP to zero when $T_a < 0\,^{\circ}\mathrm{C}$ as

$$f(T_a) = \frac{1}{1 + e^{(2(T_0 - T_a))}} \tag{3}$$

where T_0 is the inflection point (Kolari et al., 2014).

R was estimated as

$$R = R_C Q_{10}^{T_{sa}/10} \tag{4}$$

where R_C is the respiration at a reference temperature (T=0 °C), Q_{10} is the temperature sensitivity of R and T_{sa} is the mean of the air temperature at 18 m height and soil temperature at 5 cm depth. T_{sa} has been found to be a good choice as the respiration driver at Hyytiälä forest in previous studies (Kolari et al., 2009; Lasslop et al., 2012).

Parameters α, P_{max} and R_C were estimated for 11-day periods while Q_{10} was estimated from the weighted mean of monthly Q_{10} values from June–August over several years. Weights were the inverse of the confidence interval of each Q_{10} estimate. Θ was determined as the value that gave the best model fit when the partitioning was run over the summer months (June–August) over several years (Kulmala et al., 2019).

2.3.2 GPP from artificial neural networks

GPP_{ANN} from data driven model was estimated by applying the $NN_{C\text{-part}}$ algorithm (Tramontana et al., 2020). $NN_{C\text{-part}}$ is a customized neural network that emulates the bio-physical processes driving both GPP and R at ecosystem spatial scale and was applied to several vegetation types distributed globally. The network is composed by two subnetworks: one used to simulate GPP fluxes and the other one for R. The two subnetworks are joined together in the last node of the overall structure in which, the GPP and R signals were combined to calculate NEE. The subnetwork simulating GPP was composed by three layers and it estimated the ecosystem level gross photosynthesis by applying a light use efficiency (LUE) approach; in particular instantaneous LUE was estimated by the first two layers while GPP was finally calculated as the product between LUE and shortwave incoming radiation in the third layer.

Each subnetwork rely on specific predictors. Characteristics that distinguish the model are a) GPP and R derived by other models are not used, b) functional relationships are derived directly from the data and c) the network's weights are tuned by

training the machine learning only on NEE measurements. In this experiment we used the same predictors (VPD, incoming

145 shortwave radiation, potential incoming radiation, T_a, T_{soil}, SWC, wind speed and wind direction) and network structure as applied in Tramontana et al. (2020). However, to assure the operability of the method, which is limited by the availability of both predictors and NEE measurements, we set lower requirements concerning the minimum percentage of measured data for both predictors and half hourly NEE. Moreover, data from all available years were put together in the same dataset to be used in a unique "multi-years" training process. In particular, we applied the following setting: for each year, less than 55%

150 of predictors were gap-filled and at least 365 half hourly NEE should be measured for both nighttime and daytime. Despite high percentage of missing data in observations, gaps had generally short duration with limited effects on the uncertainty of predicted outputs. The final GPP$_{ANN}$ products were derived by applying trained networks on meteorological inputs, and thus do not include NEE data after network training.

2.3.3 GPP from COS flux measurements

155 Based on previous soil chamber measurements it was known that the soil COS flux at Hyytiälä forest site varies only by 1 pmol m^{-2} s^{-1} during the growing season and the diurnal variation is negligible (Kooijmans et al., 2019; Sun et al., 2018a). An average soil flux of -2.7 pmol m^{-2} s^{-1} was thus first subtracted from the quality filtered and gap-filled COS EC fluxes in order to only account for the vegetation contribution to the ecosystem COS exchange. GPP was then calculated from the ecosystem COS fluxes (FCOS) using formula (Sandoval-Soto et al., 2005; Blonquist et al., 2011)

$$160 \quad \text{GPP}_{\text{COS}} = \frac{-FCOS}{\text{LRU}} \frac{[CO_2]_a}{[COS]_a} \tag{5}$$

where $[CO_2]_a$ and $[COS]_a$ denote the atmospheric concentrations of CO$_2$ and COS (in mol m^{-3}) measured by the QCL, respectively. LRU (-) was calculated as a function of PAR (LRU$_{PAR}$) as described by the empirical equation presented in Kooijmans et al. (2019):

$$\text{LRU}_{\text{PAR}} = \frac{607.26}{PAR} + 0.57 \tag{6}$$

165 This LRU equation was based on field measurements of branch CO$_2$ and COS fluxes in 2017 at the same site and were thus independent from the EC flux measurements (Kooijmans et al., 2019).

A new theoretical LRU estimate (LRU$_{CAP}$) was developed based on the stomatal optimization model CAP (Dewar et al., 2018). The LRU$_{CAP}$ formulation was based on the following general expression for LRU given by Eqs. (10-11) of Wohlfahrt

170 et al. (2012):

$$\text{LRU} = \frac{1}{1 - \frac{c_i}{c_a}} \frac{\frac{1}{1.21} + \frac{1}{1.14} \frac{g_s^{COS}}{g_b^{COS}}}{1 + \frac{g_s^{COS}}{g_b^{COS}} + \frac{g_s^{COS}}{g_m^{COS}}} \tag{7}$$

where $g_x^{COS}(x=b,s,m)$ are, respectively, the boundary layer, stomatal and mesophyll conductances for COS, c_a is the atmospheric CO_2 molar mixing ratio (mol mol^{-1}), c_i is the leaf intercellular CO_2 molar mixing ratio (mol mol^{-1}), and the numerical factors 1.21 and 1.14 are the ratios of the conductances of CO_2 to COS for stomata and the boundary layer (Wohlfahrt et al., 2012). If it is assumed that the boundary layer and mesophyll conductances are infinite (as done by Dewar et al. (2018)), Eq. (7) reduces to

$$\text{LRU} = \frac{1}{1.21} \left(1 - \frac{c_i}{c_a} \right)^{-1}. \tag{8}$$

An analytical expression for c_i was derived from the stomatal optimization model CAP by Dewar et al. (2018), according to which stomatal conductance maximise leaf photosynthesis, reflecting a trade-off between stomatal limitations to CO_2 diffusion and non-stomatal limitations (NSLs) to carboxylation capacity. The CAP model predicts the value of c_i as an analytical function of various environmental and physiological factors. Inserting this function into Eq. (8), LRU$_{\text{CAP}}$ can then be expressed as

$$\text{LRU}_{\text{CAP}} = \frac{1}{1.21} \frac{c_a}{c_a - \Gamma^*} \left(1 + \sqrt{\frac{K_{sl}|\psi_c|}{1.6 g_c VPD}} \sqrt{1 + \frac{2\Gamma^* g_c}{\alpha PAR}} \right), \tag{9}$$

where Γ^* is the CO_2 photorespiratory compensation point (mol mol^{-1}), K_{sl} the soil-to-leaf hydraulic conductance (mol m^{-2} s^{-1} MPa^{-1}), ψ_c is the assumed critical leaf water potential (MPa) at which NSLs reduce photosynthesis to zero, g_c is the carboxylation conductance in the absence of NSLs (mol m^{-2} s^{-1}) and α is the photosynthetic quantum yield (mol mol^{-1}) in the absence of NSLs (Duursma et al., 2008; Dewar et al., 2018). While Γ^* and α vary seasonally with temperature (Bernacchi et al., 2001; Leverenz and Öquist, 1987), we decided to use fixed values of 50×10^{-6} mol mol^{-1} and 0.05 mol mol^{-1}, respectively, for simplicity. In addition to PAR (mol m^{-2}s^{-1}) and VPD measurements (mol mol^{-1}), LRU$_{\text{CAP}}$ requires soil moisture measurements through the soil component of K_{sl}. All parameter definitions and values are listed in Table 1 and a more detailed derivation of Eq. (9) is given in the Appendix (Sect. A1 and A2).

3 Results and discussion

3.1 Environmental conditions

March 2013 was colder than other years (average -7.0 °C) with also a higher average PAR (207.3 μmol m^{-2} s^{-1}) and lowest soil moisture (0.23 m^3 m^{-3}) of all years (Fig. 1). May 2017 had high amounts of radiation (monthly average PAR of 478.4 μmol m^{-2}) and soil temperature was low (3.4 °C), while soil moisture and VPD were at a normal level at 0.28 m^3 m^{-3} and 0.47 kPa, respectively. July 2014 was warmer (19.0 °C) and dryer (VPD 0.88 kPa) than other years but soil moisture remained high at 0.25 m^3 m^{-3}. A clear increase in VPD and a drop in soil moisture were seen in August 2013 and 2015 when soil moisture decreased from 0.24 (0.31 in 2015) in July to 0.19 (0.24 in 2015) m^3 m^{-3} in August in 2013 and afternoon median VPD increased to 1.00 kPa in August 2013. Soil moisture in September–December in 2017 was 10 % higher than other years, while no significant differences between years were found in other environmental variables in late autumn.

Table 1. Explanations and literature values of the parameters used in the LRU$_\text{CAP}$ formulation for Hyytiälä forest. c_a was derived from the measurements in Kooijmans et al. (2019), SWC, PAR and VPD form measurements done in this study, other values are from Dewar et al. (2018), Duursma et al. (2008), (Bernacchi et al., 2001) and Nikinmaa et al. (2013). Soil-related values ($K_{soil,sat}$, r_{cyl}, SWC_{sat} and b) are for soil horizon B (which was considered to be representative of the rooting zone), where the SWC measurements were also made. Values measured at the site are written in bold.

Symbol	Definition	Default value or formula and unit
c_a	Atmospheric CO_2 molar mixing ratio	415×10^{-6} mol mol^{-1}
Γ^*	Photorespiratory compensation point of CO_2	50×10^{-6} mol mol^{-1}
g_c	Carboxylation conductance in the absence of non-stomatal limitations	0.5 mol m^{-2} s^{-1}
ψ_c	Critical leaf water potential	-2 MPa
α	Photosynthetic quantum yield	0.05 mol mol^{-1}
K_{sl}	Leaf-specific soil-to-leaf hydraulic conductance	$\frac{K_{soil} K_x}{K_{soil} + K_x}$; mol m^{-2}s^{-1}MPa^{-1}
K_x	Leaf-specific root-to-leaf xylem hydraulic conductance	0.78×10^{-3} mol m^{-2}s^{-1}MPa^{-1}
K_{soil}	Leaf-specific soil hydraulic conductance	$\frac{R_1}{\text{LAI}} \frac{2\pi k_{soil}}{\log\left(\frac{r_{cyl}}{r_{root}}\right)}$; mol m^{-2}s^{-1}MPa^{-1}
k_{soil}	Soil hydraulic conductivity	$k_{soil,sat} \left(\frac{\textbf{SWC}}{SWC_{sat}}\right)^{2b+3}$; mol m^{-1}s^{-1}MPa^{-1}
$k_{soil,sat}$	Saturated soil hydraulic conductivity	5.7 mol m^{-1}s^{-1}MPa^{-1}
R_1	Root length index	5300 m^{-1}
LAI	Leaf area index, all-sided	8 m^{2}m^{-2}
r_{cyl}	Radius of the cylinder of soil accessible to a root	0.00458 m
r_{root}	Fine root radius	0.3×10^{-3} m
SWC_{sat}	Saturation soil water content	0.52 m^3 m^{-3}
SWC	Soil water content	m^3 m^{-3}
b	Parameter of the soil water retention curve	4.46
VPD	Vapor pressure deficit	mol mol^{-1}
PAR	Photosynthetically active radiation	mol m^{-2}s^{-1}

3.2 GPP comparison from sub-daily to seasonal scales

GPP$_\text{ANN}$ showed slightly higher midday values than GPP$_\text{NLR}$ during summer months (May–July) in 2014 and 2017 (Figs. 2,3,4a), opposite to what was found in Tramontana et al. (2020) when comparing GPP$_\text{ANN}$ to standard FLUXNET partitioning during summer months for multiple sites. The difference during other months was negligible. We tested how the more widely
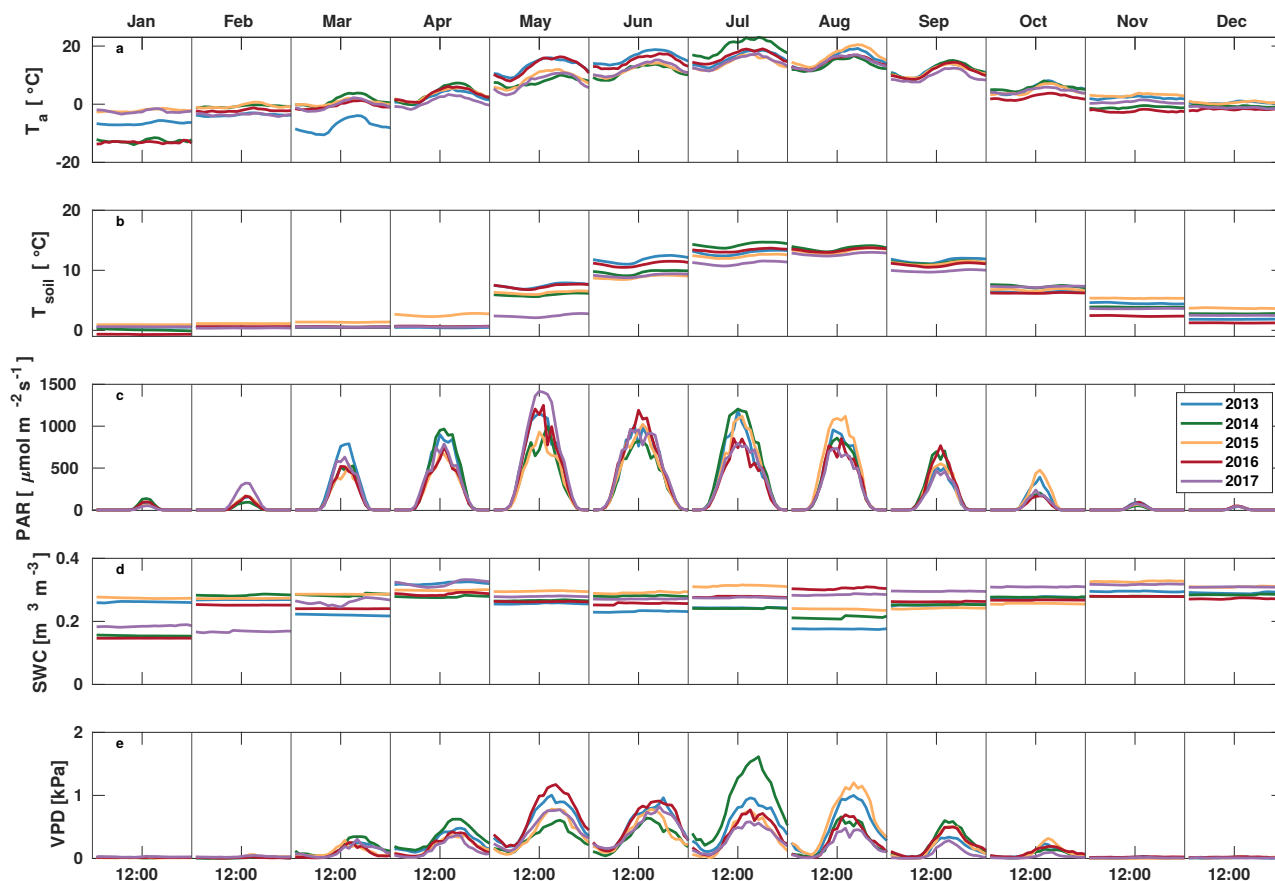
Figure 1. Median diurnal variation of T_a, T_{soil}, PAR, SWC and VPD in different months during the measurement period 2013–2017.

used partitioning method of using only air temperature as the respiration driver, GPP$_{airT}$, (instead of the average of soil and air temperatures) would perform against GPP$_{NLR}$ and found the two methods to agree very well with each other at all time scales studied (Fig. B1). The small differences in the diurnal variations of GPP$_{NLR}$ and GPP$_{ANN}$ are thus not due to the chosen temperature measurement as respiration driver. During the measurement period 2013–2017, daily GPP$_{ANN}$ did not differ from GPP$_{NLR}$ statistically (tested with Student's t-test). However, at 30 min time scale the GPP$_{ANN}$ was on average 15 % lower than GPP$_{NLR}$. The lower agreement of 30 min GPP$_{ANN}$ and GPP$_{NLR}$ than at longer time scales may result from the NN$_{C-part}$ method restricting GPP$_{ANN}$ to only positive values while GPP$_{NLR}$ may have even negative values due to random noise in the NEE measurements. The relative and absolute differences of GPP$_{ANN}$ to GPP$_{NLR}$ are, however, very small when averaging over longer time periods (Fig. 5).

GPP$_{COS,PAR}$ performed very similarly to GPP$_{NLR}$ especially during morning and early evening (Fig. 2,3), but showed higher midday values than GPP$_{NLR}$, especially during summer months (May–August) in all years. At the daily scale, GPP$_{COS,PAR}$

was on average 23 % higher than GPP$_{\text{NLR}}$ (Figs. 4d,5) and also differed from GPP$_{\text{NLR}}$ statistically (p<0.01) as tested with Student's t-test.

To investigate further the causes of the higher GPP$_{\text{COS,PAR}}$, we tried another LRU approach based on a stomatal conductance model, LRU$_{\text{CAP}}$ (Sect. 2.3.3). LRU$_{\text{CAP}}$ uses PAR, SWC and VPD as well as ecosystem specific literature values for some
220 parameters as input variables, while LRU$_{\text{PAR}}$ by Kooijmans et al. (2019) only uses PAR. LRU$_{\text{CAP}}$ could potentially better take into account e.g. the effects of drought on stomatal control. In spring, the diurnal variation of GPP$_{\text{COS,CAP}}$ follows closely those of GPP$_{\text{NLR}}$ and GPP$_{\text{ANN}}$ until June (Fig. 2, 3). Especially in June and July GPP$_{\text{COS,CAP}}$ is lower than the other GPP estimates. At 30 min time scale GPP$_{\text{COS,CAP}}$ is on average 12 % lower than GPP$_{\text{NLR}}$, but there is large scatter due to noisy FCOS measurements, as in GPP$_{\text{COS,PAR}}$. However, there is less scatter in GPP$_{\text{COS,CAP}}$ than GPP$_{\text{COS,PAR}}$, indicating that
225 some of the scatter is due to LRU estimation. At daily scale GPP$_{\text{COS,CAP}}$ is 7% higher than GPP$_{\text{NLR}}$ and at monthly scale the difference decreases to 3%. However, there is no statistically significant difference between the daily values of GPP$_{\text{NLR}}$ and GPP$_{\text{COS,CAP}}$, as tested with Student's t-test. The relative and absolute difference of GPP$_{\text{COS,CAP}}$ to GPP$_{\text{NLR}}$ is also mostly lower than that of GPP$_{\text{COS,PAR}}$ to GPP$_{\text{NLR}}$ throughout the year (Fig. 5). In addition, GPP$_{\text{COS,CAP}}$ finds the same two distinctive probability density function peaks as GPP$_{\text{NLR}}$ and GPP$_{\text{ANN}}$ at 1.7 and 6.6 μmol m^{-2}s^{-1} while GPP$_{\text{COS,PAR}}$
230 finds weaker peaks at 2.4 and 7.4 μmol m^{-2}s^{-1} (Fig. 6). It can be thus said, that GPP$_{\text{COS,CAP}}$ gives a better agreement with traditional GPP$_{\text{NLR}}$ partitioning than GPP$_{\text{COS,PAR}}$. However, it was noted that LRU$_{\text{CAP}}$ was overestimated at high radiation (PAR > 1000 μmol m^{-2}s^{-1}, Fig. B2a).

LRU$_{\text{CAP}}$ was also calculated based on a combination of literature values and fitted parameters (Sect. A1) by fitting parameters $X = \frac{|\psi_c|}{1.6 g_c}$ and $Y = \frac{2\Gamma^* g_c}{\alpha}$ to Eq. (9). This exercise allows for better analysis of the uncertainties of LRU$_{\text{CAP}}$. While
235 literature values would give $X = 2.5$ and $Y = 0.001$, the fitting resulted in $X = 2.64$ and $Y = 0.0033$ and a better agreement of LRU$_{\text{CAP}}$ with measured LRU (RMSE=1.89, while without fitting RMSE=2.01). While X was close to its literature value, Y was estimated three times higher. This mismatch suggests there may be scope for further model improvement, such as the inclusion of dark respiration and/or finite mesophyll conductance in the LRU$_{\text{CAP}}$ model. However, as the difference between fitted LRU$_{\text{CAP}}$ and LRU$_{\text{CAP}}$ with only literature values was not large and the applicability of the model without fitting is
240 better, we decided to use the literature value-based LRU$_{\text{CAP}}$ in this study, without fitting to measured LRU.

LRU$_{\text{CAP}}$ was also calculated assuming finite mesophyll conductance as a test (Sect. A2). The agreement of this method was better than assuming infinite mesophyll conductance at high PAR, but worse at low PAR (Fig. B2d), very similar to the results from Maignan et al. (2021), who modelled LRU at Hyytiälä using the ORCHIDEE model. This version of LRU$_{\text{CAP}}$ was also fitted to measured LRU in terms of parameters X and Y (Sect. A2) to make the low PAR LRU$_{\text{CAP}}$ better, which resulted in
245 $X = 3.45$ and $Y = 0.0057$, both higher than their expected literature values. We thus concluded that the assumption of infinite g_m is more valid. Kooijmans et al. (2019) found that internal conductance (a combination of mesophyll conductance and biochemical reactions) might limit leaf-scale FCOS during daytime. We find a better agreement of LRU$_{\text{CAP}}$ with measured LRU if g_m is assumed infinite, but there is a mismatch at high PAR, supporting the possibility that g_m might indeed be a limiting factor under high radiation.

Table 2. Cumulative GPP (gC m^{-2}) over May–July with different GPP estimates. All sums are calculated from same data coverage and the fraction of gap-filled flux data (CO_2 flux for GPP_{NLR}, COS flux for $GPP_{COS,PAR}$ and $GPP_{COS,CAP}$) is presented in parentheses. GPP_{ANN} does not include gap-filled NEE data, since it is based on meteorological variables. *In 2015, the cumulative sum covers only July.

Year	GPP_{NLR}	GPP_{ANN}	$GPP_{COS,PAR}$	$GPP_{COS,CAP}$
2013	481 (0.16)	473	597 (0.28)	510 (0.28)
2014	294 (0.20)	324	414 (0.24)	343 (0.24)
2015	193 (0.23)*	188*	212 (0.31)*	165 (0.31)*
2016	623 (0.40)	565	722 (0.43)	599 (0.43)
2017	387 (0.35)	399	522 (0.34)	428 (0.34)

250   All cumulative GPP estimates over May–July (Table 2) were about half of the yearly GPP reported previously (Lagergren et al., 2008; Ilvesniemi et al., 2009; Kolari et al., 2009; Suni et al., 2003), since we did not measure GPP over the whole growing season (that lasts c. 30 weeks) but only 13 weeks around the peak growing season. Cumulative $GPP_{COS,PAR}$ was (on average 25 %) higher than cumulative GPP_{NLR} in all studied years. This is higher than the 4.3 % difference reported in Spielmann et al. (2019) and 3.5 % agreement reported in Commane et al. (2015). Cumulative $GPP_{COS,CAP}$ on the other hand varied from 17 %

255   higher in 2014 to 15 % lower in 2015 being on average only 3 % higher than cumulative GPP_{NLR}. Cumulative GPP_{ANN} varied from 10 % higher in 2014 to 9 % lower in 2016 than GPP_{NLR}, on average being 0.1 % lower than GPP_{NLR}. As stated above, overall GPP_{ANN} was closest to GPP_{NLR} from the three GPP estimates. $GPP_{COS,CAP}$ was closer to both of the CO_2-based GPP estimates than $GPP_{COS,PAR}$. However, at high PAR, $LRU_{COS,CAP}$ was overestimated in comparison to observations, leading to underestimated GPP. Still, no firm conclusions can be drawn on this as the LRU observations only cover measurements at

260   the top of the canopy, and may not reflect LRU over the whole canopy.

It has been suggested that, due to the Kok effect, leaf respiration is inhibited under radiation (Kok, 1949). This inhibition has been estimated to be approximately 13 % in the evergreen needle-leaf forests during summer (Keenan et al., 2019). Isotopic studies measuring the CO_2 isotope fluxes have come to the conclusion that due to the Kok effect, the traditional GPP from CO_2 flux partitioning using the nighttime method is overestimated and isotopic flux measurements support this statement

265   (Wehr et al., 2016). However, the ecosystem respiration at the Hyytiälä forest site is dominated by soil respiration (Ilvesniemi et al., 2009), which could limit the importance of the Kok effect in this ecosystem (Keenan et al. (2019); Yin et al. (2020)). Reduced leaf respiration under radiation would be visible as a break point around the compensation point with a change of the slope of NEE against radiation. However, such a break point was not detected in our observations, as is demonstrated in Fig. B3. It is thus not expected that independent GPP estimates in Hyytiälä would necessarily result in lower GPP than the

270   traditional methods. Moreover, as demonstrated in Tramontana et al. (2020), the uncertainties and biases in NEE (and COS flux) measurements exceed those resulting from the possible Kok effect.
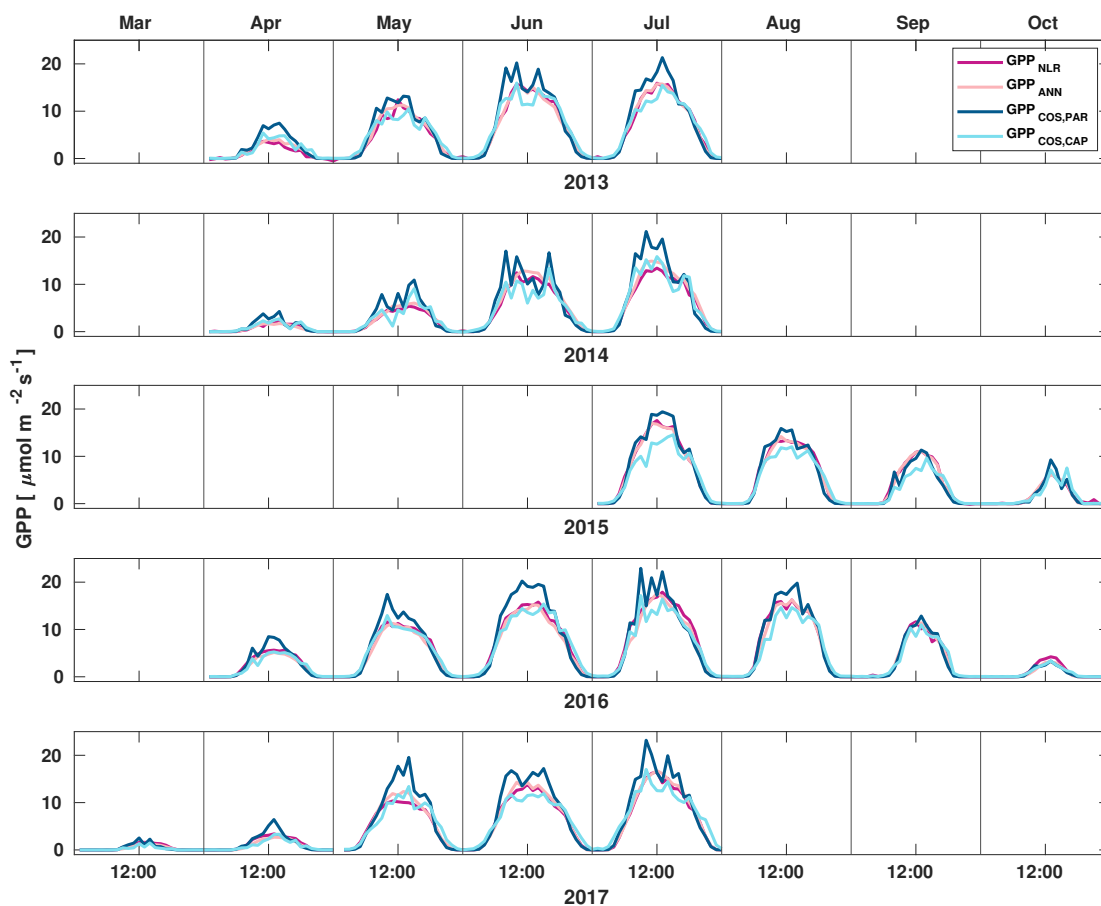
Figure 2. Median diurnal variation of traditionally paritITioned GPP (GPP$_{\mathrm{NLR}}$, purple line), GPP from artificial neural networks (GPP$_{\mathrm{ANN}}$, pink line), GPP from COS flux measurements with LRU determined according to Kooijmans et al. (2019) (GPP$_{\mathrm{COS,PAR}}$, dark blue line) and GPP from COS flux measurements using a new approach for LRU (Sect. 2.3.3, GPP$_{\mathrm{COS,CAP}}$, light blue line) in different months during the measurement period 2013–2017. Averaging was done to the same data points and only months with more than 55 % of data coverage were included.

3.3 GPP responses to environmental conditions

All four GPP estimates responded similarly to environmental forcing (PAR, T_a, VPD) both in spring and summer (Fig. 7). In spring, all GPP estimates increased with increasing radiation levels, while in summer a saturation point was found at PAR>500

275 μmol m^{-2}s^{-1}. GPP$_{\mathrm{COS,PAR}}$ was higher than GPP$_{\mathrm{COS,CAP}}$ at PAR>400 μmol m^{-2}s^{-1} while at low PAR values they agreed well with each other both in spring and summer, as well as with GPP$_{\mathrm{NLR}}$ and GPP$_{\mathrm{ANN}}$. GPP$_{\mathrm{COS,PAR}}$ thus has a stronger
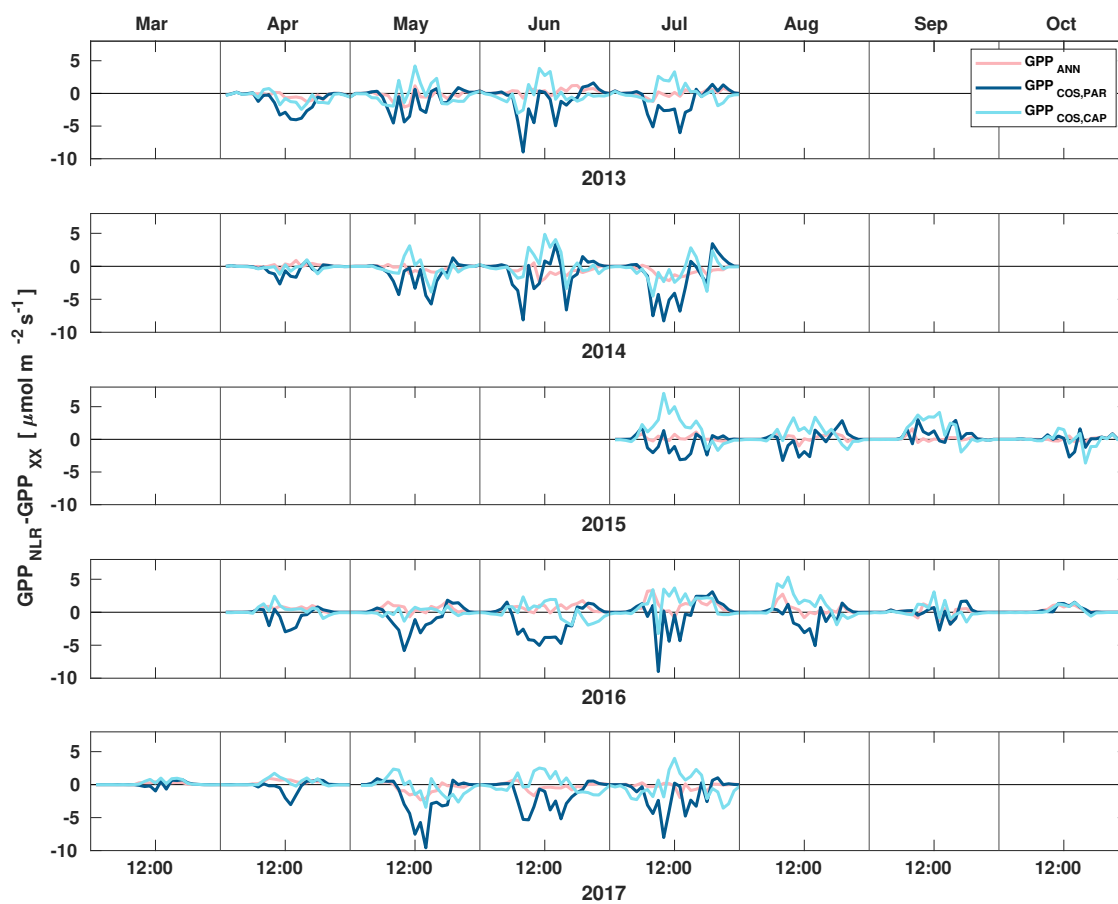
Figure 3. Diurnal variation of the difference of GPP$_{\text{ANN}}$ (pink), GPP$_{\text{COS,PAR}}$ (dark blue) and GPP$_{\text{COS,CAP}}$ (light blue) to the reference GPP$_{\text{NLR}}$ in different months during the measurement period 2013–2017. Averaging was done to the same data points and only months with more than 55 % of data coverage were included.

radiation response than the other GPP estimates. A similar PAR response was found in Spielmann et al. (2019), who studied GPP$_{\text{COS,PAR}}$ with a traditional GPP partitioning method in four different sites in Europe. Although GPP$_{\text{COS,CAP}}$ agrees well with both GPP$_{\text{NLR}}$ and GPP$_{\text{ANN}}$ at high PAR, it is likely underestimated due to overestimated LRU$_{\text{CAP}}$ at high PAR.

280   In spring, increasing air temperature increased all GPP estimates similarly until T_a reached 17°C. However, again GPP$_{\text{COS,PAR}}$ was higher than other GPP estimates. In summer, air temperature did not have a notable effect on any GPP estimate. Responses to VPD were similar for each GPP estimates both in spring and summer. In spring, decreasing air humidity (increasing VPD) was increasing GPP until VPD>0.7 kPa after which VPD did not have an effect. In summer, dryness started to limit GPP at
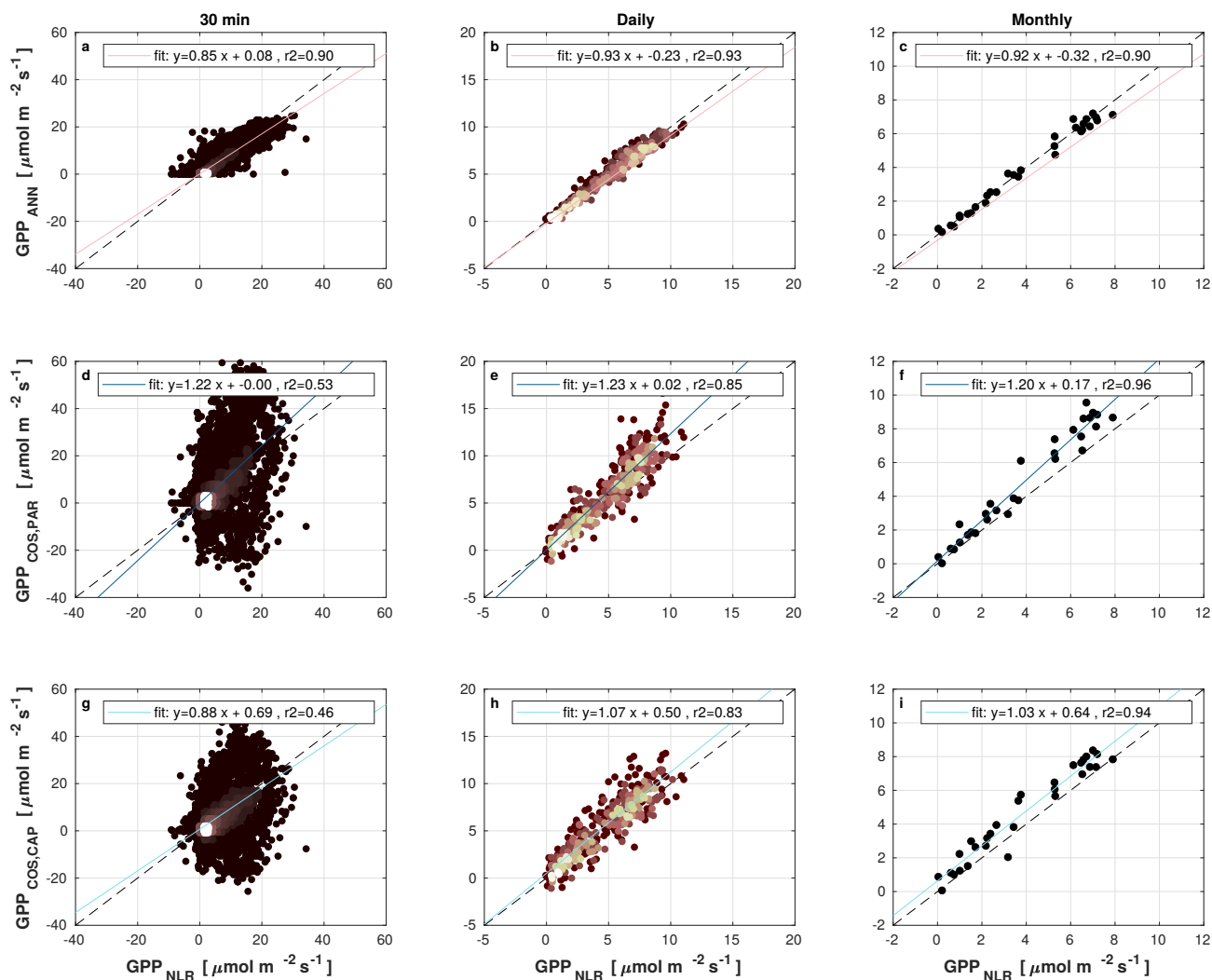
Figure 4. Scatter plots of GPP$_{ANN}$, GPP$_{COS,PAR}$ and GPP$_{COS,CAP}$ against GPP$_{NLR}$ in 30 min, daily and monthly time scales. The color of data points in 30 min and daily scatter plots indicate the data density, lighter colors indicating higher point density than dark.

VPD>1 kPa. We found that similar to PAR and T_a responses, GPP$_{COS,PAR}$ was higher than other GPP estimates at low VPD

285 values, but decreased to similar levels at high VPD (1 kPa) both in spring and summer.

Wohlfahrt et al. (2018) used FCOS to determine whether a reduction in GPP during a heatwave is due to diffusional or biochemical limitations, because FCOS tracks the diffusional limitations only while CO_2 flux is a combination of both. As we did not observe drought or heatwaves in Hyytiälä during the measurement period, we cannot assess the effects of drought to GPP$_{COS,PAR}$ or GPP$_{COS,CAP}$. We can, however, see that GPP$_{COS,PAR}$ gives higher GPP at low VPD than the CO_2-based
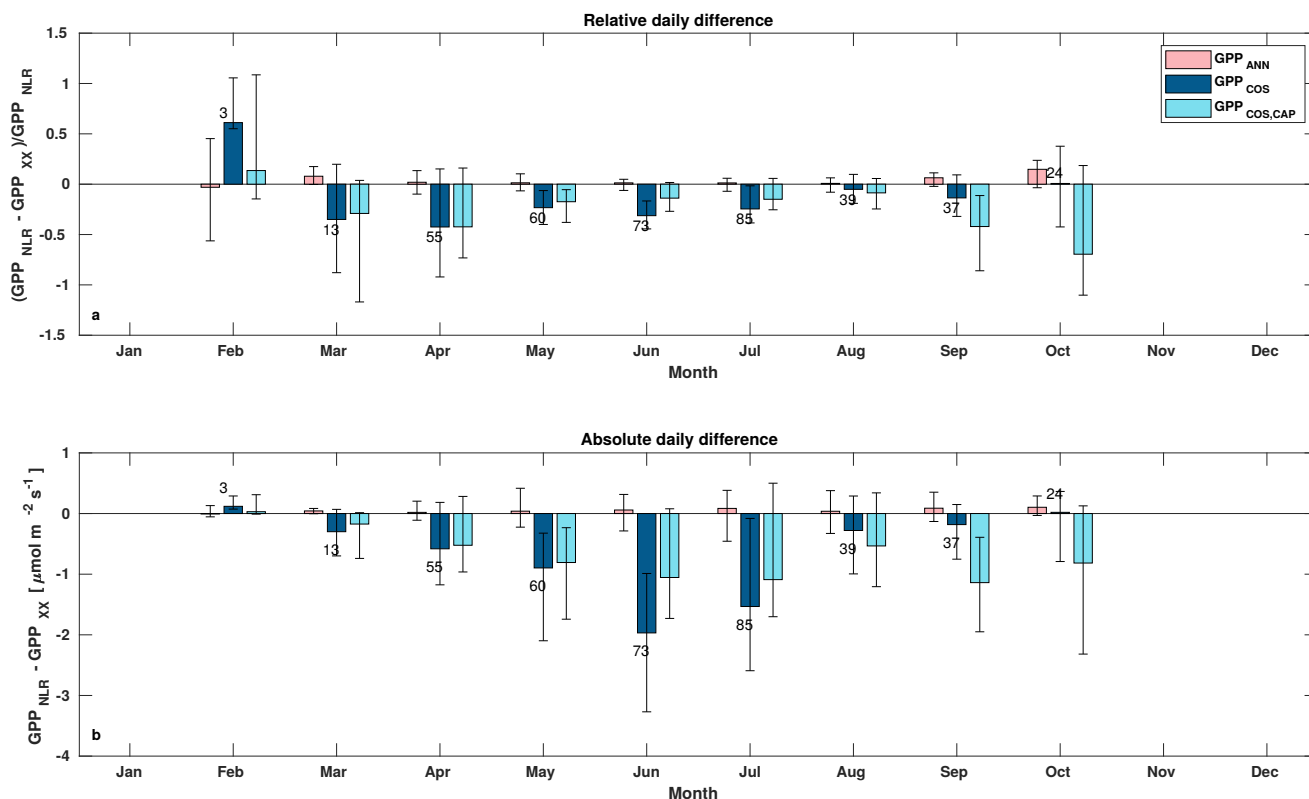
Figure 5. Relative (a) and absolute (b) difference of daily GPP$_{\text{ANN}}$ (pink), GPP$_{\text{COS,PAR}}$ (dark blue) and GPP$_{\text{COS,CAP}}$ (light blue) to GPP$_{\text{NLR}}$ in different months, averaged over the whole measurement period 2013–2017. Bars represent the median difference, and whiskers show the 25th and 75th percentiles. Numbers on top of the bars indicate how many daily flux data points have been used for calculating the medians. All medians have been calculated using the same number of data points.

290   methods, as does GPP$_{\text{COS,CAP}}$ in spring (Fig. 7). This may indicate that something is limiting the photosynthesis reaction (e.g. biochemical limitations in CO_2 assimilation) even though the diffusion into the leaf is not limited.

3.4   Uncertainties and limitations of the GPP methods

Because GPP$_{\text{ANN}}$ is purely based on data, it has high sensitivity to the uncertainty in the input data. Moreover, it is sensitive

295   to missing data especially in the case of long data gaps (Tramontana et al., 2020). The method also requires large data sets for training NN$_{\text{C−part}}$, not available at all measurement sites. However, GPP$_{\text{ANN}}$ does not require prescribed relationships of GPP to environmental data making it an attractive method for sites with good data availability.

     GPP$_{\text{COS,PAR}}$ uses an empirical PAR relation that is based on measurements done at Hyytiälä forest. This relation should be tested against branch scale COS and CO_2 flux measurements at other sites, as a different PAR relation was found in Yang et al.
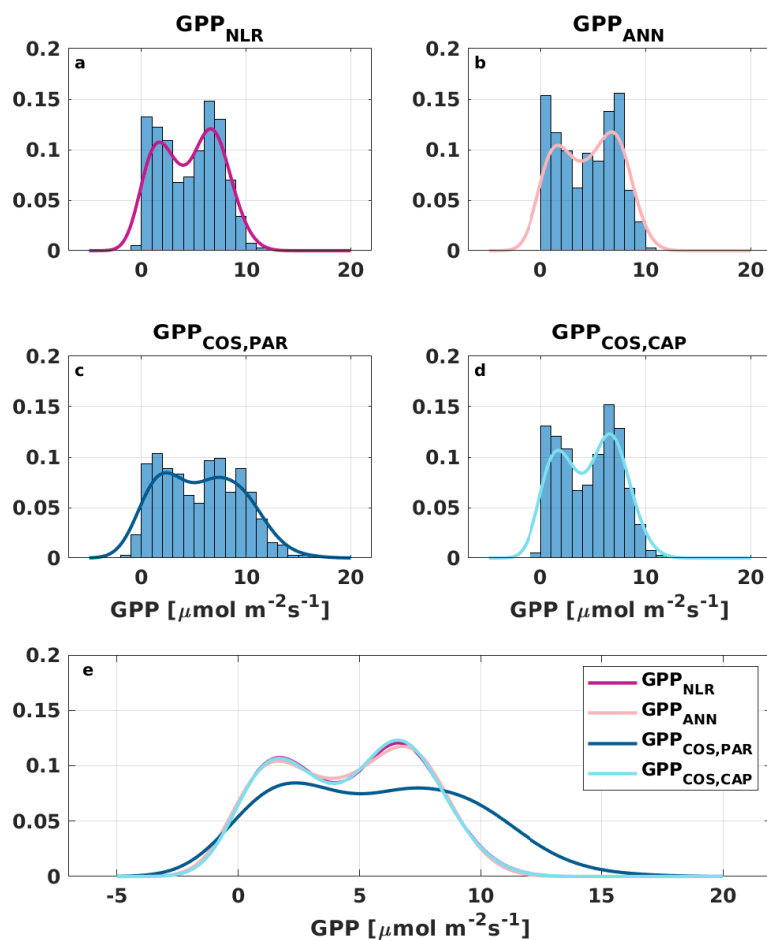
Figure 6. Distribution (bars) and probability density functions (lines) of daily average (a) GPP_{NLR}, (b) GPP_{ANN}, (c) $GPP_{COS,PAR}$ and (d) $GPP_{COS,CAP}$. All probability density functions are combined in (e) for better comparison.

300 (2018) and it is not known if this relation holds elsewhere. While the LRU_{PAR} function is simple, and in that sense attractive, it does not take into account e.g. stomatal regulation during drought or non-stomatal limitations. Moreover, as an empirical fit, it does not provide process-based understanding for LRU. While the results of $GPP_{COS,PAR}$ are promising, we observed a difference similar to what was found in Kooijmans et al. (2019) and did not find as good agreement with CO_2-based GPP estimates as Asaf et al. (2013), who found an agreement within 15% between these two methods using a constant LRU of 1.6

305 in Mediterranean pine forests and crop fields. However, they also reported higher GPP_{COS} assumed to be related to soil COS uptake, which was not measured or taken into account in GPP calculations in their study. In our study, we have subtracted an average measured soil flux (Sun et al., 2018a) from the ecosystem COS uptake. The diurnal variation in soil COS flux
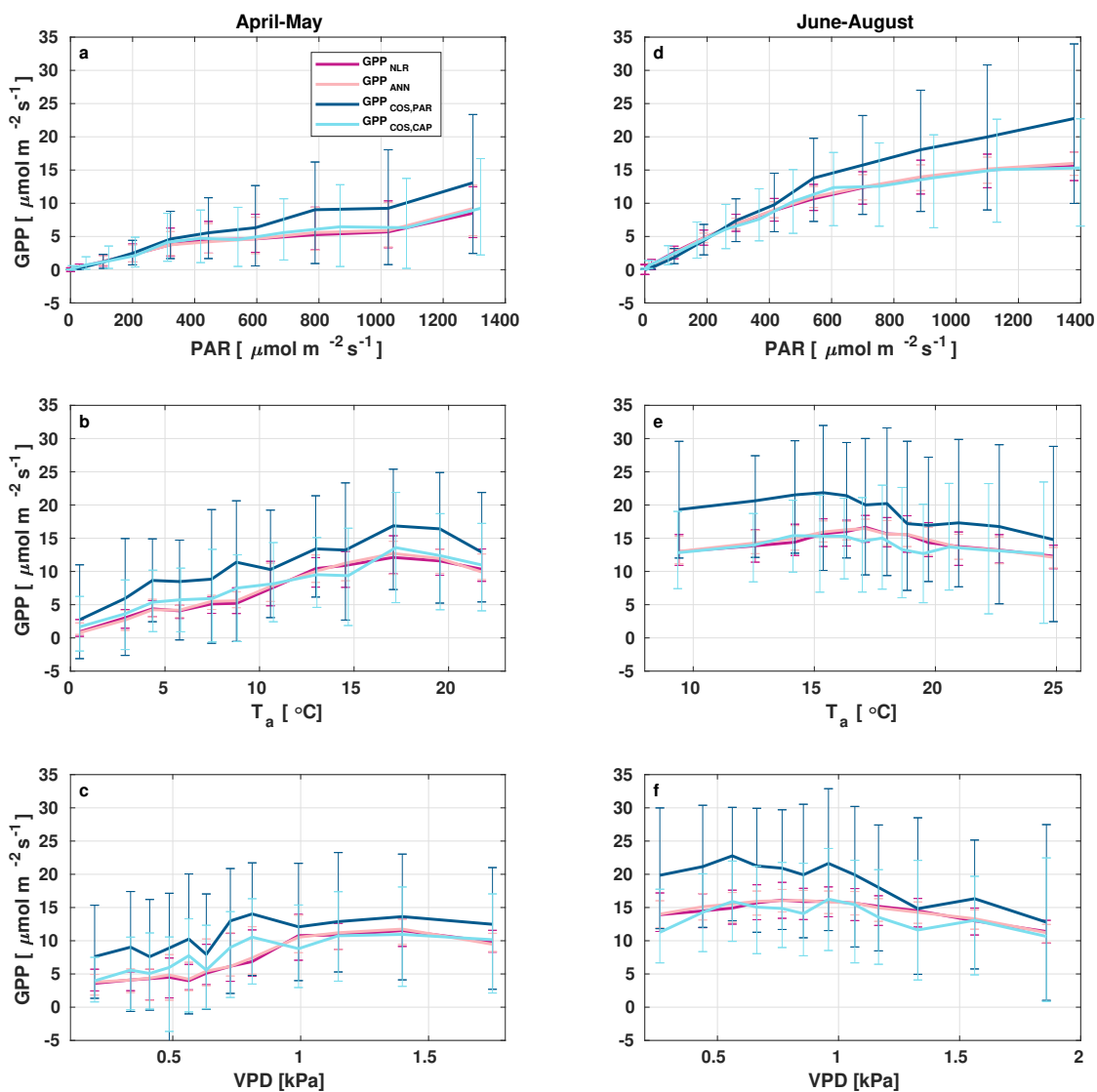
Figure 7. Responses of the different GPP estimates (GPP$_{NLR}$ (purple), GPP$_{ANN}$ (pink), GPP$_{COS,PAR}$ (dark blue) and GPP$_{COS,CAP}$, light blue) to environmental parameters – photosynthetically active radiation (a,d), air temperature (b,e) and vapor pressure deficit (c,f) – in spring (a–c) and summer (d–f). Data are binned to 12 equal sized bins (same number of data points in each bin) and all GPPs have the same data coverage. Only measured (non-gap-filled) 30 min flux data was used and GPP was filtered to include only PAR>700 μmol m^{2}s^{-1} in responses to T_a and VPD to avoid simultaneous correlation with PAR.

was small (less than 1 pmol m^{-2}s^{-1}) throughout the season, so averaging did not make a large difference and thus soil does not explain the differences found here. However, as soil COS flux measurements are not necessarily available at all sites, this

310 may be one source of uncertainty in wider application. Yang et al. (2018) studied COS flux components and GPP$_{\mathrm{COS}}$ in a Mediterranean citrus orchard and found GPP$_{\mathrm{COS}}$ to be on average 7 % lower than traditionally partitioned GPP. They also presented a light-dependent and seasonally varying LRU which, however, could not be applied to Hyytiälä COS fluxes due to the very different ecosystem types studied, indicating that the PAR responses may differ between ecosystems.

GPP$_{\mathrm{COS,CAP}}$ could be more applicable at other sites than GPP$_{\mathrm{COS,PAR}}$ due to the use of only literature values and simple

315 meteorological variables in LRU$_{\mathrm{CAP}}$ without requiring fits to measured LRU. However, as LRU$_{\mathrm{PAR}}$, LRU$_{\mathrm{CAP}}$ should also be tested at other sites as well against measured LRU to verify its applicability at other ecosystems. Moreover, this version of LRU$_{\mathrm{CAP}}$ assumes infinite mesophyll conductance, which may be a limiting factor of the method. We also provide a formulation of LRU$_{\mathrm{CAP}}$ with finite g_m, which was not comparable to measured LRU at Hyytiälä forest, but could be so at other measurement sites.

320 One source of uncertainty in both of the LRU approaches is that they are based on measurements on top of the canopy where there is no foliage blocking the incoming radiation. The branch chamber measurements (which the parameterized LRU$_{\mathrm{PAR}}$ function is based on) were done at the top of the canopy and the LRU$_{\mathrm{CAP}}$ model is also based on top of the canopy. The measured needles were thus well-adjusted to high radiation conditions and the radiation measurements used in both LRU calculations are also only from above the canopy. Therefore, we did not take into account the light penetration and scatter

325 through canopy. However, the needles and leaves within the canopy are also well adjusted to low light conditions and may be more efficient with their stomatal control in varying light conditions than the needles on top of the canopy. Thus, we do not assume this to be a large source of uncertainty.

4 Conclusions

Daily GPP$_{\mathrm{ANN}}$ did not statistically differ from daily GPP$_{\mathrm{NLR}}$ and differences were very small also in the sub-daily and seasonal

330 scales. We found that GPP$_{\mathrm{COS,PAR}}$ was in general higher than GPP$_{\mathrm{NLR}}$ at all time scales studied, including a cumulative GPP estimate over a three-month period during the peak growing season. Instead, a better agreement was found between the newly introduced GPP$_{\mathrm{COS,CAP}}$ and GPP$_{\mathrm{NLR}}$ at all time scales. GPP$_{\mathrm{COS,CAP}}$ was also less scattered at 30 min time scale than GPP$_{\mathrm{COS,PAR}}$. Moreover, the new LRU$_{\mathrm{CAP}}$ function provides a new, theoretical formulation for COS-based GPP estimates that can be used at other measurement locations as well, ideally without additional branch chamber measurements. This is

335 vast improvement from the previous LRU functions that are site-specific empirical fits. However, the LRU$_{\mathrm{CAP}}$ model still overestimates LRU at high radiation, when compared to LRU observations at the top of the canopy, leading to an underestimated GPP$_{\mathrm{COS,CAP}}$ at midday, especially in summer. This may result from the assumption of infinite mesophyll conductance or the lack of dark respiration in the CAP stomatal optimization model, on which LRU$_{\mathrm{CAP}}$ is based. All GPP estimates were close to values reported earlier for Hyytiälä. Both COS-based GPP estimates suggest a higher GPP than the CO$_2$-based methods

340 at longer time scales. The new LRU$_{\mathrm{CAP}}$ model development would benefit from further testing at other measurement sites

with COS and CO_2 branch flux measurements, including measurements inside the canopy for better canopy-integrated LRU estimates. The COS-based GPP estimates provide an opportunity for better process-based understanding of photosynthesis, rather than a method applicable everywhere, since the COS flux measurements are noisier, expensive and more difficult than those of CO_2. In addition to COS, other proxies, such as solar induced fluorescence and isotopic flux measurements should

345 be tested simultaneously to properly investigate their deficiencies and advantages in estimating GPP and processes underlying photosynthesis.

Data availability. Environmental data used in the study are available in the AVAA – Open research data publishing platform (https://smear. avaa.csc.fi/). The metadata of the observations are available via the Etsin service. Flux data will be published in a public repository before publication.

Appendix A: LRU predicted by the CAP stomatal optimization model

A1 LRU$_{\mathrm{CAP}}$ assuming infinite mesophyll conductance

The general expression for the leaf relative uptake ratio (LRU) according to Wohlfahrt et al. (2012) is

$$\mathrm{LRU} = \frac{1}{1 - \frac{c_i}{c_a}} \frac{\frac{1}{1.21} + \frac{1}{1.14}\frac{g_s^{COS}}{g_b^{COS}}}{1 + \frac{g_s^{COS}}{g_b^{COS}} + \frac{g_s^{COS}}{g_m^{COS}}}. \tag{A1}$$

where $g_x^{COS}(x = b, s, m)$ are the boundary layer, stomatal and mesophyll conductances for COS, respectively, c_a is the atmospheric, c_i the leaf intercellular CO_2 molar mixing ratio (mol mol^{-1}), and the numerical factors 1.21 and 1.14 are the ratios of the conductances of CO_2 to COS for stomata and the boundary layer (Wohlfahrt et al., 2012).

If it is assumed that boundary layer and mesophyll conductances are infinite, Eq. (A1) reduces to

$$\mathrm{LRU} = \frac{1}{1.21}\left(1 - \frac{c_i}{c_a}\right)^{-1} \tag{A2}$$

$$= \frac{1}{1.21}\frac{c_a}{\hat{c}_a}\left(1 - \frac{\hat{c}_i}{\hat{c}_a}\right)^{-1} \tag{A3}$$

where $\hat{c}_i \equiv c_i - \Gamma^*$, $\hat{c}_a \equiv c_a - \Gamma^*$ and Γ^* is the photorespiratory compensation point of CO_2 (mol mol^{-1}). c_i was found from a stomatal optimization model in which the CAP optimization hypothesis is applied to the bi-substrate photosynthesis model as in Dewar et al. (2018). The bi-substrate photosynthesis model is closely based on the one presented by Thornley and Johnson (1990) in their Eq. (9.12i). The CAP solution for stomatal conductance (Dewar et al., 2018) predicts

$$\frac{\hat{c}_i}{\hat{c}_a} = \frac{1}{1+\beta}, \tag{A4}$$

where

$$\beta = \sqrt{\frac{1.6D}{K_{sl}|\psi_c|}\left(\frac{1}{g_c} + \frac{2\Gamma^*}{\alpha Q}\right)^{-1}}, \tag{A5}$$

where D is vapor pressure deficit (VPD; mol mol^{-1}), K_{sl} is the leaf-specific soil-to-leaf hydraulic conductance (mol m^{-2}s^{-1}MPa^{-1}), ψ_c is the assumed critical leaf water potential (MPa) at which non-stomatal limitations (NSLs) reduce photosynthesis to zero, g_c is the carboxylation conductance in the absence of NSLs (mol m^{-2} s^{-1}), α is the photosynthetic quantum yield (mol mol^{-1}) in the absence of NSLs and Q is the photosynthetically active radiation (PAR; mol m^{-2}s^{-1}). Substituting Eqs. (A4) and (A5) and the definition of $\hat{c}_a$ into Eq. (A3) gives

$$\mathrm{LRU}_{\mathrm{CAP}} = \frac{1}{1.21}\frac{c_a}{\hat{c}_a}\left(1 + \frac{1}{\beta}\right) \tag{A6}$$

$$= \frac{1}{1.21}\frac{c_a}{c_a - \Gamma^*}\left(1 + \sqrt{\frac{K_{sl}|\psi_c|}{1.6Dg_c}}\sqrt{1 + \frac{2\Gamma^*g_c}{\alpha Q}}\right). \tag{A7}$$

In addition to purely using literature values in $\mathrm{LRU_{CAP}}$, some of the parameters were also fitted in order to analyze the deficiencies of the model. In particular, two fitting parameters $X = \frac{|\psi_c|}{1.6 g_c}$ and $Y = \frac{2\Gamma^* g_c}{\alpha}$ were assigned so that Eq. (A7) became

$$\mathrm{LRU_{CAP}} = \frac{1}{1.21} \frac{c_a}{c_a - \Gamma^*} \left(1 + \sqrt{\frac{K_{sl} X}{D}} \sqrt{1 + \frac{Y}{Q}} \right). \tag{A8}$$

Parameters X and Y were then optimized to minimize the RMSE of $\log(\mathrm{LRU_{CAP}})$ to measured $\log(\mathrm{LRU})$, due to the logarithmic nature of LRU, with Matlab's $fminsearch$ function.

A2 $\mathrm{LRU_{CAP}}$ assuming finite mesophyll conductance

In the case that mesophyll conductance is not assumed infinite, but boundary layer conductance is, Eq. (A1) becomes

$$\mathrm{LRU} = \frac{1}{1.21} \frac{1}{1 + \frac{g_s^{COS}}{g_m^{COS}}} \left(1 - \frac{c_i}{c_a} \right)^{-1}. \tag{A9}$$

Further assuming the ratios of stomatal to mesophyll conductance same for CO_2 and COS and knowing that $g_s^{CO2}(c_a - c_i) = g_m^{CO2}(c_i - c_c)$, where c_c is the chloroplast CO_2 molar mixing ratio (mol mol^{-1}), we get

$$\frac{g_s^{COS}}{g_m^{COS}} = \frac{g_s^{CO2}}{g_m^{CO2}} = \frac{c_i - c_c}{c_a - c_i}. \tag{A10}$$

Implementing Eq. (A10) into Eq. (A9) gives

$$\mathrm{LRU} = \frac{1}{1.21} \left(1 - \frac{c_c}{c_a} \right)^{-1} \tag{A11}$$

$$= \frac{1}{1.21} \frac{c_a}{c_a - \Gamma^*} \left(1 - \frac{\hat{c}_c}{\hat{c}_a} \right)^{-1}. \tag{A12}$$

The CAP model predicts the optimal stomatal conductance by maximizing the rate of leaf photosynthesis A (Dewar et al., 2018). In the case that mesophyll conductance is finite and non-stomatal limitations act entirely on g_m with no effect on the biochemical efficiencies, A is given by

$$A = \frac{\alpha Q g_c (c_c - \Gamma^*)}{\alpha Q + g_c (c_c + \Gamma^*)}. \tag{A13}$$

This equation can be used to calculate the value of c_c:

$$\hat{c}_c \equiv c_c - \Gamma^* = \frac{\left(\frac{\alpha Q}{g_c} + 2\Gamma^* \right) A}{\alpha Q - A} \tag{A14}$$

into which we can then substitute the CAP solution for A. The CAP solution for stomatal conductance is given by Dewar et al. (2018) as

$$g_s = \frac{\alpha Q}{\frac{\alpha Q}{g_c} + 2\Gamma^*} \frac{x\theta}{x\beta^2 + (1-x)(xw+1)} \tag{A15}$$

where

$$\theta = 1 - \frac{\psi_{soil}}{\psi_c} \tag{A16}$$

$$w = \frac{c_a - \Gamma^*}{\frac{\alpha Q}{g_c} + 2\Gamma^*} \tag{A17}$$

$$x = \frac{c_i - \Gamma^*}{c_a - \Gamma^*} = \frac{1}{1+\beta} \tag{A18}$$

where ψ_{soil} is the saturated soil water potential (MPa). Substituting x as a function of β and simplifying gives

$$g_s = \frac{\alpha Q}{\frac{\alpha Q}{g_c} + 2\Gamma^*} \frac{\theta}{\beta(1 + \beta + \frac{w}{1+\beta})}. \tag{A19}$$

We then find the CAP solution for A as follows

$$A = g_s(c_a - c_i) = g_s(\hat{c}_a - \hat{c}_i) \tag{A20}$$

$$= g_s \hat{c}_a (1-x) \tag{A21}$$

$$= g_s \hat{c}_a \frac{\beta}{1+\beta} \tag{A22}$$

$$= \frac{\alpha Q \hat{c}_a}{\frac{\alpha Q}{g_c} + 2\Gamma^*} \frac{\theta}{(1+\beta)^2 + w}. \tag{A23}$$

Substituting this into Eq. (A14) and simplifying then gives

$$\frac{\hat{c}_c}{\hat{c}_a} = \frac{\theta}{(1+\beta)^2 + (1-\theta)w} \tag{A24}$$

$$= \frac{\theta}{(1+\beta)^2 + (1-\theta)\frac{g_c(c_a - \Gamma^*)}{\alpha Q + 2\Gamma^* g_c}} \tag{A25}$$

that can finally be substituted into Eq. (A12) for the solution of $\mathrm{LRU_{CAP}}$ with finite mesophyll conductance.

Similar to $\mathrm{LRU_{CAP}}$ with infinite mesophyll conductance, this formulation was also fitted in terms of X and Y. In the parameterization, β and w were expressed in terms of X and Y so that

$$\beta = \frac{1}{\sqrt{\frac{K_{sl}X}{D}\left(1 + \frac{Y}{Q}\right)}} \tag{A26}$$

and

$$w = \frac{c_a - \Gamma^*}{2\Gamma^*} \frac{1}{\frac{Q}{Y} + 1} \tag{A27}$$

and implemented into Eq. (A24).

Appendix B: Additional figures
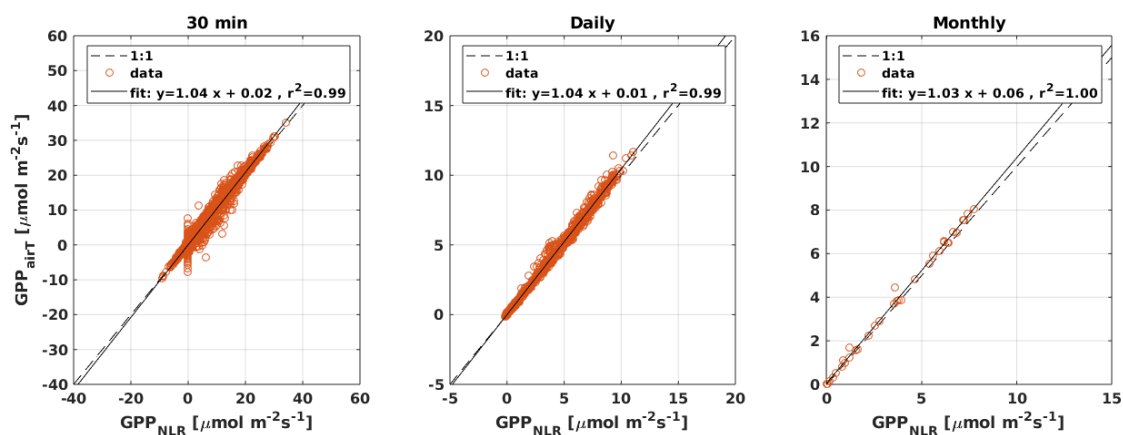
Figure B1. Scatter plots of GPP$_{\mathrm{airT}}$ that uses only air temperature as the driver for respiration against GPP$_{\mathrm{NLR}}$ that uses an average of air and soil temperatures as the respiration driver in 30 min, daily and monthly time scales. Black line is the least-squares linear fit to the data.
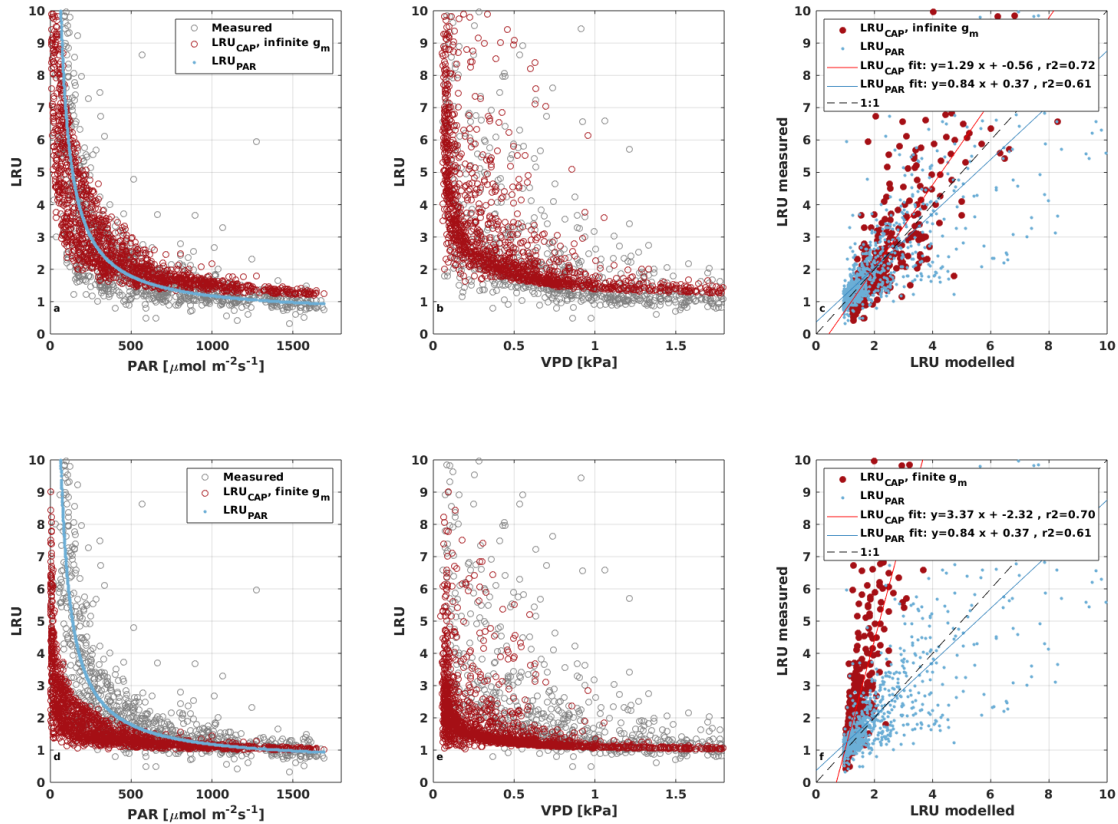
Figure B2. Measured LRU (gray) and modelled LRU_{PAR} (blue) and LRU_{CAP} (red) assuming infinite (a-c) or finite (d-f) mesophyll conductance (g_m) in LRU_{CAP} against PAR and VPD. Subplots c and d compare the measured LRU against modelled LRU_{PAR} and LRU_{CAP}.
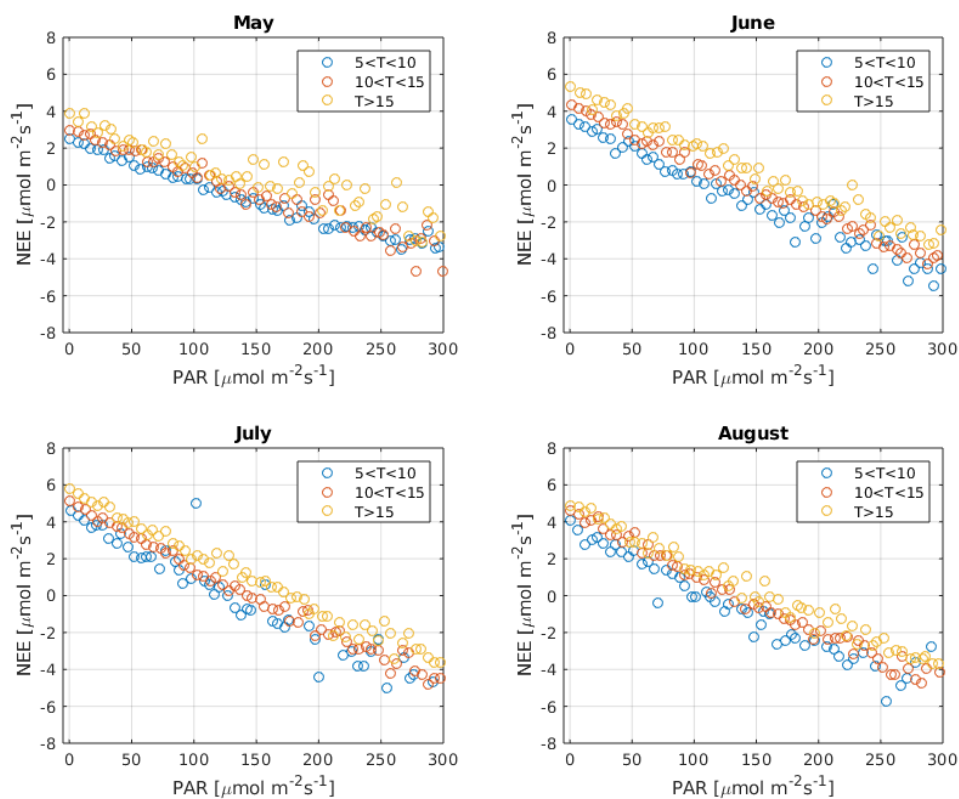
Figure B3. Net ecosystem exchange (NEE) against photosynthetically active radiation (PAR) close to the compensation point during May, June, July and August. Data are binned to different air temperature classes: $5°C < T_a < 10°C$ (blue), $10°C < T_a < 15°C$ (orange) and $T_a > 15°C$ (yellow).

420 *Author contributions.* KMK, IM and TV designed the study. KMK, PK and LMJK performed the measurements and flux processing. RD, AM and KMK developed the new LRU formulation. GT provided the GPP estimate by artificial neural networks. All authors contributed by commenting the study design, results and the manuscript. KMK wrote the manuscript with contributions from all co-authors.

Competing interests. The authors declare that they have no conflict of interest.

Acknowledgements. Special thanks to Helmi Keskinen, Sirpa Rantanen, Janne Levula, and other Hyytiälä technical staff for all their support
425 with the measurements. The authors thank the Academy of Finland Centre of Excellence (118780), Academy Professor projects (312571 and 282842), ICOS Finland (3119871), ACCC Flagship funded by the Academy of Finland grant number 337549, Academy of Finland project 342930 and the Tyumen region government in accordance with the Program of the World-Class West Siberian Interregional Scientific and Educational Center (National Project "Nauka"). KMK thanks the Vilho, Yrjö and Kalle Väisälä foundation for its support. GT would like to acknowledge the support from the European Research Council (ERC) under the ERC-2017-STG SENTIFLEX project (grant agreement
430 755617). LMJK was supported by the ERC advanced funding scheme (AdG 2016, project no. 742798, project abbreviation COS-OCS). DP thanks the E-SHAPE H2020 project (grant agreement 820852) and the ICOS-ETC.

References

Asaf, D., Rotenberg, E., Tatarinov, F., Dicken, U., Montzka, S. A., and Yakir, D.: Ecosystem photosynthesis inferred from measurements of carbonyl sulphide flux, Nature Geoscience, 6, 186–190, https://doi.org/10.1038/NGEO1730, 2013.

435 Aubinet, M.: Eddy covariance CO_2 flux measurements in nocturnal conditions: an analysis of the problem, Ecological Applications, 18, 1368–1378, 2008.

Bernacchi, C., Singsaas, E., Pimentel, C., Portis Jr, A., and Long, S.: Improved temperature response functions for models of Rubisco-limited photosynthesis, Plant, Cell & Environment, 24, 253–259, https://doi.org/10.1111/j.1365-3040.2001.00668.x, 2001.

Berry, J., Wolf, A., Campbell, J. E., Baker, I., Blake, N., Blake, D., Denning, A. S., Kawa, S. R., Montzka, S. A., Seibt, U., Stimler, K., Yakir,

440 D., and Zhu, Z.: A coupled model of the global cycles of carbonyl sulfide and CO_2 : A possible new window on the carbon cycle, Journal of Geophysical Research: Biogeosciences, 118, 842–852, https://doi.org/10.1002/jgrg.20068, 2013.

Blonquist, J. M., Montzka, S. A., Munger, J. W., Yakir, D., Desai, A. R., Dragoni, D., Griffis, T. J., Monson, R. K., Scott, R. L., and Bowling, D. R.: The potential of carbonyl sulfide as a proxy for gross primary production at flux tower sites, Journal of Geophysical Research, 116, https://doi.org/10.1029/2011JG001723, 2011.

445 Commane, R., Meredith, L., Baker, I. T., Berry, J. A., Munger, J. W., and Montzka, S. A.: Seasonal fluxes of carbonyl sulfide in a midlatitude forest, Proceedings of the National Academy of Sciences, 112, 14 162—-14 167, https://doi.org/10.1073/pnas.1504131112, 2015.

Desai, A., Richardson, A., Moffat, A., Kattge, J., Hollinger, D., Barr, A., Falge, E., Noormets, A., Papale, D., Reichstein, M., and Stauch, V.: Cross-site evaluation of eddy covariance GPP and RE decomposition techniques, Agricultural and Forest Meteorology, 148, 821–838, https://doi.org/https://doi.org/10.1016/j.agrformet.2007.11.012, 2008.

450 Dewar, R., Mauranen, A., Mäkelä, A., Hölttä, T., Medlyn, B., and Vesala, T.: New insights into the covariation of stomatal, mesophyll and hydraulic conductances from optimization models incorporating nonstomatal limitations to photosynthesis, New Phytologist, 217, 571–585, https://doi.org/https://doi.org/10.1111/nph.14848, 2018.

Dusenge, M. E., Duarte, A. G., and Way, D. A.: Plant carbon metabolism and climate change: elevated CO_2 and temperature impacts on photosynthesis, photorespiration and respiration, New Phytologist, 221, 32–49, 2019.

455 Duursma, R. A., Kolari, P., Perämäki, M., Nikinmaa, E., Hari, P., Delzon, S., Loustau, D., Ilvesniemi, H., Pumpanen, J., and Mäkelä, A.: Predicting the decline in daily maximum transpiration rate of two pine stands during drought based on constant minimum leaf water potential and plant hydraulic conductance, Tree physiology, 28, 265–276, 2008.

Friedlingstein, P., O'sullivan, M., Jones, M. W., Andrew, R. M., Hauck, J., Olsen, A., Peters, G. P., Peters, W., Pongratz, J., Sitch, S., Le Quéré, C., Canadell, J. G., Ciais, P., Jackson, R. B., Alin, S., Aragão, L. E. O. C., Arneth, A., Arora, V., Bates, N. R., Becker, M., Benoit-Cattin,

460 A., Bittig, H. C., Bopp, L., Bultan, S., Chandra, N., Chevallier, F., Chini, L. P., Evans, W., Florentie, L., Forster, P. M., Gasser, T., Gehlen, M., Gilfillan, D., Gkritzalis, T., Gregor, L., Gruber, N., Harris, I., Hartung, K., Haverd, V., Houghton, R. A., Ilyina, T., Jain, A. K., Joetzjer, E., Kadono, K., Kato, E., Kitidis, V., Korsbakken, J. I., Landschützer, P., Lefèvre, N., Lenton, A., Lienert, S., Liu, Z., Lombardozzi, D., Marland, G., Metzl, N., Munro, D. R., Nabel, J. E. M. S., Nakaoka, S.-I., Niwa, Y., O'Brien, K., Ono, T., Palmer, P. I., Pierrot, D., Poulter, B., Resplandy, L., Robertson, E., Rödenbeck, C., Schwinger, J., Séférian, R., Skjelvan, I., Smith, A. J. P., Sutton, A. J., Tanhua, T., Tans,

465 P. P., Tian, H., Tilbrook, B., van der Werf, G., Vuichard, N., Walker, A. P., Wanninkhof, R., Watson, A. J., Willis, D., Wiltshire, A. J., Yuan, W., Yue, X., and Zaehle, S.: Global carbon budget 2020, Earth System Science Data, 12, 3269–3340, 2020.

Hari, P. and Kulmala, M.: Station for Measuring Ecosystem–Atmosphere Relations (SMEAR II), Boreal Environment Research, 10, 315–322, 2005.

Heskel, M. A., Atkin, O. K., Turnbull, M. H., and Griffin, K. L.: Bringing the Kok effect to light: a review on the integration of daytime
470   respiration and net ecosystem exchange, Ecosphere, 4, 1–14, 2013.

Ilvesniemi, H., Levula, J., Ojansuu, R., Kolari, P., Kulmala, L., Pumpanen, J., Launiainen, S., Vesala, T., and Nikinmaa, E.: Long-term
        measurements of the carbon balance of a boreal Scots pine dominated forest ecosystem, Boreal Environment Research, 14, 731–753,
        2009.

Keenan, T. F., Migliavacca, M., Papale, D., Baldocchi, D., Reichstein, M., Torn, M., and Wutzler, T.: Widespread inhibition of daytime
475   ecosystem respiration, Nature ecology & evolution, 3, 407–415, 2019.

Kettle, A. J., Kuhn, U., Von Hobe, M., Kesselmeier, J., and Andreae, M. O.: Global budget of atmospheric carbonyl sulfide:
        Temporal and spatial variations of the dominant sources and sinks, Journal of Geophysical Research: Atmospheres, 107, 1–16,
        https://doi.org/10.1029/2002JD002187, 2002.

Kohonen, K.-M., Kolari, P., Kooijmans, L., Chen, H., Seibt, U., Sun, W., and Mammarella, I.: Towards standardized processing of eddy
480   covariance flux measurements of carbonyl sulfide, Atmospheric Measurement Techniques, 13, 3957–3975, https://doi.org/10.5194/amt-
        13-3957-2020, 2020.

Kok, B.: On the interrelation of respiration and photosynthesis in green plants, Biochimica et biophysica acta, 3, 625–631, 1949.

Kolari, P., Kulmala, L., Pumpanen, J., Launiainen, S., Ilvesniemi, H., Hari, P., and Nikinmaa, E.: CO_2 exchange and component CO_2 fluxes
        of a boreal Scots pine forest, 14, 761–783, 2009.

485   Kolari, P., Chan, T., Porcar-Castell, A., Bäck, J., Nikinmaa, E., and Juurola, E.: Field and controlled environment measurements show
        strong seasonal acclimation in photosynthesis and respiration potential in boreal Scots pine, Frontiers in plant science, 5, 717,
        https://doi.org/https://doi.org/10.3389/fpls.2014.00717, 2014.

Kooijmans, L. M., Sun, W., Aalto, J., Erkkilä, K.-M., Maseyk, K., Seibt, U., Vesala, T., Mammarella, I., and Chen, H.: Influences of light
        and humidity on carbonyl sulfide-based estimates of photosynthesis, Proceedings of the National Academy of Sciences, 116, 2470–2475,
490   2019.

Kulmala, L., Pumpanen, J., Kolari, P., Dengel, S., Berninger, F., Köster, K., Matkala, L., Vanhatalo, A., Vesala, T., and Bäck, J.: Inter-and
        intra-annual dynamics of photosynthesis differ between forest floor vegetation and tree canopy in a subarctic Scots pine stand, Agricultural
        and Forest Meteorology, 271, 1–11, https://doi.org/10.1016/j.agrformet.2019.02.029, 2019.

Lagergren, F., Lindroth, A., Dellwik, E., Ibrom, A., Lankreijer, H., Launiainen, S., Mölder, M., Kolari, P., Pilegaard, K., and Vesala, T.:
495   Biophysical controls on CO_2 fluxes of three Northern forests based on long-term eddy covariance data, Tellus B: Chemical and Physical
        Meteorology, 60, 143–152, 2008.

Lasslop, G., Reichstein, M., Papale, D., Richardson, A., Arneth, A., Barr, A., Stoy, P., and Wohlfahrt, G.: Separation of net ecosystem
        exchange into assimilation and respiration using a light response curve approach: critical issues and global evaluation, Global Change
        Biology, 16, 187–208, 2010.

500   Lasslop, G., Migliavacca, M., Bohrer, G., Reichstein, M., Bahn, M., Ibrom, A., Jacobs, C., Kolari, P., Papale, D., Vesala, T., Wohlfahrt,
        G., and Cescatti, A.: On the choice of the driving temperature for eddy-covariance carbon dioxide flux partitioning, Biogeosciences, 9,
        5243–5259, https://doi.org/10.5194/bg-9-5243-2012, 2012.

Launois, T., Belviso, S., Bopp, L., Fichot, C. G., and Peylin, P.: A new model for the global biogeochemical cycle of carbonyl sulfide - Part
        1: Assessment of direct marine emissions with an oceanic general circulation and biogeochemistry model, Atmospheric Chemistry and
505   Physics, 15, 2295–2312, https://doi.org/10.5194/acp-15-2295-2015, 2015.

Leverenz, J. and Öquist, G.: Quantum yields of photosynthesis at temperatures between-; 2°C and 35°C in a cold-tolerant C3 plant (Pinus sylvestris) during the course of one year, Plant, Cell & Environment, 10, 287–295, 1987.

Luo, Y., Keenan, T., and Smith, M.: Predictability of the terrestrial carbon cycle, Global change biology, 21, 1737–1751, 2015.

Maignan, F., Abadie, C., Remaud, M., Kooijmans, L. M. J., Kohonen, K.-M., Commane, R., Wehr, R., Campbell, J. E., Belviso, S., Montzka,
510   S. A., Raoult, N., Seibt, U., Shiga, Y. P., Vuichard, N., Whelan, M. E., and Peylin, P.: Carbonyl sulfide: comparing a mechanistic representation of the vegetation uptake in a land surface model and the leaf relative uptake approach, Biogeosciences, 18, 2917–2955, https://doi.org/10.5194/bg-18-2917-2021, 2021.

Mammarella, I., Peltola, O., Nordbo, A., Järvi, L., and Rannik, Ü.: Quantifying the uncertainty of eddy covariance fluxes due to the use of different software packages and combinations of processing steps in two contrasting ecosystems, Atmospheric Measurement Techniques,
515   9, 4915–4933, https://doi.org/10.5194/amt-9-4915-2016, 2016.

Montzka, S., Calvert, P., Hall, B., Elkins, J., Conway, T., Tans, P., and Sweeney, C.: On the global distribution, seasonality, and budget of atmospheric carbonyl sulfide (COS) and some similarities to CO_2, Journal of Geophysical Research: Atmospheres, 112, 2007.

Nikinmaa, E., Hölttä, T., Hari, P., Kolari, P., Mäkelä, A., Sevanto, S., and Vesala, T.: Assimilate transport in phloem sets conditions for leaf gas exchange, Plant, Cell & Environment, 36, 655–669, 2013.

520   Papale, D., Reichstein, M., Aubinet, M., Canfora, E., Bernhofer, C., Kutsch, W., Longdoz, B., Rambal, S., Valentini, R., Vesala, T., and Yakir, D.: Towards a standardized processing of Net Ecosystem Exchange measured with eddy covariance technique: algorithms and uncertainty estimation, Biogeosciences, 3, 571–583, 2006.

Piao, S., Ciais, P., Friedlingstein, P., Peylin, P., Reichstein, M., Luyssaert, S., Margolis, H., Fang, J., Barr, A., Chen, A., Grelle, A., Hollinger, D., Laurila, T., Lindroth, A., Richardson, A., and Vesala, T.: Net carbon dioxide losses of northern ecosystems in response to autumn
525   warming, Nature, 451, 49–52, https://doi.org/https://doi.org/10.1038/nature06444, 2008.

Protoschill-Krebs, G., Wilhelm, C., and Kesselmeier, J.: Consumption of carbonyl sulphide (COS) by higher plant carbonic anhydrase (CA), Atmospheric Environment, 30, 3151–3156, 1996.

Reichstein, M., Falge, E., Baldocchi, D., Papale, D., Aubinet, M., Berbigier, P., Bernhofer, C., Buchmann, N., Gilmanov, T., Granier, A., Grünwald, T., Havránková, K., Ilvesniemi, H., Janous, D., Knohl, A., Laurila, T., Lohila, A., Loustau, D., Matteucci, G., Meyers, T.,
530   Miglietta, F., Ourcival, J. M., Pumpanen, J., Rambal, S., Rotenberg, E., Sanz, M., Tenhunen, J., Seufert, G., Vaccari, F., Vesala, T., Yakir, D., and Valentini, R.: On the separation of net ecosystem exchange into assimilation and ecosystem respiration: Review and improved algorithm, Global Change Biology, 11, 1424–1439, https://doi.org/10.1111/j.1365-2486.2005.001002.x, 2005.

Sandoval-Soto, L., Stanimirov, M., Von Hobe, M., Schmitt, V., Valdes, J., Wild, A., and Kesselmeier, J.: Global uptake of carbonyl sulfide (COS) by terrestrial vegetation: Estimates corrected by deposition velocities normalized to the uptake of carbon dioxide (CO_2),
535   Biogeosciences, 2, 125–132, 2005.

Spielmann, F., Wohlfahrt, G., Hammerle, A., Kitz, F., Migliavacca, M., Alberti, G., Ibrom, A., El-Madany, T. S., Gerdel, K., Moreno, G., Kolle, O., Karl, T., Peressotti, A., and Delle Vedove, G.: Gross primary productivity of four European ecosystems constrained by joint CO2 and COS flux measurements, Geophysical Research Letters, 46, 5284–5293, 2019.

Stimler, K., Berry, J. A., and Yakir, D.: Effects of Carbonyl Sulfide and Carbonic Anhydrase on Stomatal Conductance, Plant Physiology,
540   158, 524–530, https://doi.org/10.1104/pp.111.185926, 2012.

Sun, W., Kooijmans, L., Maseyk, K., Chen, H., Mammarella, I., Vesala, T., Levula, J., Keskinen, H., and Seibt, U.: Soil fluxes of carbonyl sulfide (COS), carbon monoxide, and carbon dioxide in a boreal forest in southern Finland, Atmospheric Chemistry and Physics, 18, 1363–1378, 2018a.

Sun, W., Maseyk, K., Lett, C., and Seibt, U.: Stomatal control of leaf fluxes of carbonyl sulfide and CO_2 in a Typha freshwater marsh,
Biogeosciences, 15, 3277–3291, 2018b.

Suni, T., Berninger, F., Markkanen, T., Keronen, P., Rannik, Ü., and Vesala, T.: Interannual variability and timing of growing-season CO2
exchange in a boreal forest, Journal of Geophysical Research: Atmospheres, 108, 2003.

Thornley, J. and Johnson, I.: Plant and crop modelling, 1990.

Tramontana, G., Migliavacca, M., Jung, M., Reichstein, M., Keenan, T. F., Camps-Valls, G., Ogee, J., Verrelst, J., and Papale, D.: Par-
titioning net carbon dioxide fluxes into photosynthesis and respiration using neural networks, Global change biology, 26, 5235–5253,
https://doi.org/10.1111/gcb.15203, 2020.

Vesala, T., Kohonen, K.-M., Praplan, A. P., Kooijmans, L. M. J., Foltýnová, L., Kolari, P., Kulmala, M., Bäck, J., Nelson, D., Yakir, D.,
Zahniser, M., and Mammarella, I.: Long-term fluxes of carbonyl sulfide and their seasonality and interannual variability in a boreal forest,
Atmospheric Chemistry and Physics Discussions, 2021, 1–19, https://doi.org/10.5194/acp-2021-721, 2021.

Wehr, R., Munger, J., McManus, J., Nelson, D., Zahniser, M., Davidson, E., Wofsy, S., and Saleska, S.: Seasonality of temperate forest
photosynthesis and daytime respiration, Nature, 534, 680–683, 2016.

Whelan, M. E., Lennartz, S., Gimeno, T. E., Wehr, R., Wohlfahrt, G., Wang, Y., Kooijmans, L., Hilton, T. W., Belviso, S., Peylin, P.,
Commane, R., Sun, W., Chen, H., Kuai, L., Mammarella, I., Maseyk, K., Berkelhammer, M., Li, K.-F., Yakir, D., Zumkehr, A., Katayama,
Y., Ogée, J., Spielmann, F., Kitz, F., Rastogi, B., Kesselmeier, J., Marshall, J., Erkkilä, K.-M., Wingate, L., Meredith, L., He, W., Bunk,
R., Launois, T., Vesala, T., Schmidt, J., Fichot, C. G., Seibt, U., Saleska, S., Saltzman, E., Montzka, S., Berry, J. A., and Campbell, J.:
Reviews and syntheses: Carbonyl sulfide as a multi-scale tracer for carbon and water cycles, Biogeosciences, 15, 3625–3657, 2018.

Wohlfahrt, G., Brilli, F., Hörtnagl, L., Xu, X., Bingemer, H., Hansel, A., and Loreto, F.: Carbonyl sulfide (COS) as a tracer for canopy
photosynthesis, transpiration and stomatal conductance: potential and limitations, Plant, cell & environment, 35, 657–667, 2012.

Wohlfahrt, G., Gerdel, K., Migliavacca, M., Rotenberg, E., Tatarinov, F., Müller, J., Hammerle, A., Julitta, T., Spielmann, F., and Yakir, D.:
Sun-induced fluorescence and gross primary productivity during a heat wave, Scientific reports, 8, 1–9, 2018.

Yang, F., Qubaja, R., Tatarinov, F., Rotenberg, E., and Yakir, D.: Assessing canopy performance using carbonyl sulfide measurements, Global
Change Biology, 24, 3486–3498, https://doi.org/10.1111/gcb.14145, 2018.

Yin, X., Niu, Y., van der Putten, P., and Struik, P.: The Kok effect revisited, New Phytologist, 227, 1764–1775,
https://doi.org/10.1111/nph.16638, 2020.